# Problems of Planetology, Cosmochemistry and Meteoritica

**Basilevsky A.T.[1] and Yuan Li [2]. Surface morpology of permanently shadowed floors of the south-polar lunar craters Haworth, Shoemaker and Faustini.** *UDC 523.3*

[1] Vernadsky institute, RAN, 119991, Moscow, Russia, atbas@geokhi.ru
[2] Suzhou Vocational University, SuZhou, 215009, China, YuanLi_SciRes@outlook.com.

**Abstract.** Axis of the Moon rotation is almost perpendicular to the ecliptipc plane and this is why in lunar polar regions on the crater floors is a permanent shadow. It is very cold there and vapors of water and other volatiles, which are produced due to impacts of meteorites and comets, as well as in magmatic eruptions, are being condensed there. In these areas in the pores of lunar regolith are accumulated ices of volatiles, including water ice, which is interesting as a source of water for future lunar bases and as the raw material for fuel/oxidant for future flights from the Moon to other bodies of the Solar system. Using the data of laser altimeter LOLA and LROC NAC images we produced digital terrain models, which in turn were used to study surface morphology of floors of the south-pole craters Haworth (D = 51 km), Shoemaker (D = 51 km) and Faustini (D = 39 km), as well as of "normally illuminated" working area of Lunokhod-2 and Apollo-16 landing site. In all five studied regions surface morphology is dominated by impact craters with diameters smaller than 1 km. The relative depths of craters with diameters 150 to 400 m in all studied regions are approximately the same. This information is important for future exploration of the Moon.

***Keywords***: *the Moon, permanently shadowed, hill-shade image, craters, water ice, regolith*

Axis of rotation of the Moon is almost perpendicular to direction of solar rays. That is why in polar areas of the Moon the Sun is very low above the horizon and floors of craters are permanently shadowed. As a result, the surface temperature there is below 70K and these cold traps capture volatile components which are released when meteorites and comets strike the Moon and as the result of magmatic eruptions. So, in regolith of permanently shadowed areas are being accumulated ices of $H_2O$, $H_2S$, $NH_3$, $SO_2$… (see e.g., Colaprete et al., 2010). These accumulated volatiles can be interesting as a source of water for future lunar bases and as a fuel/oxidant for flights from the Moon to planets ($H_2O$ => solar energy => $H_2$ + O). And this is one of the reasons of high interest of space agencies to study polar regions of the Moon.

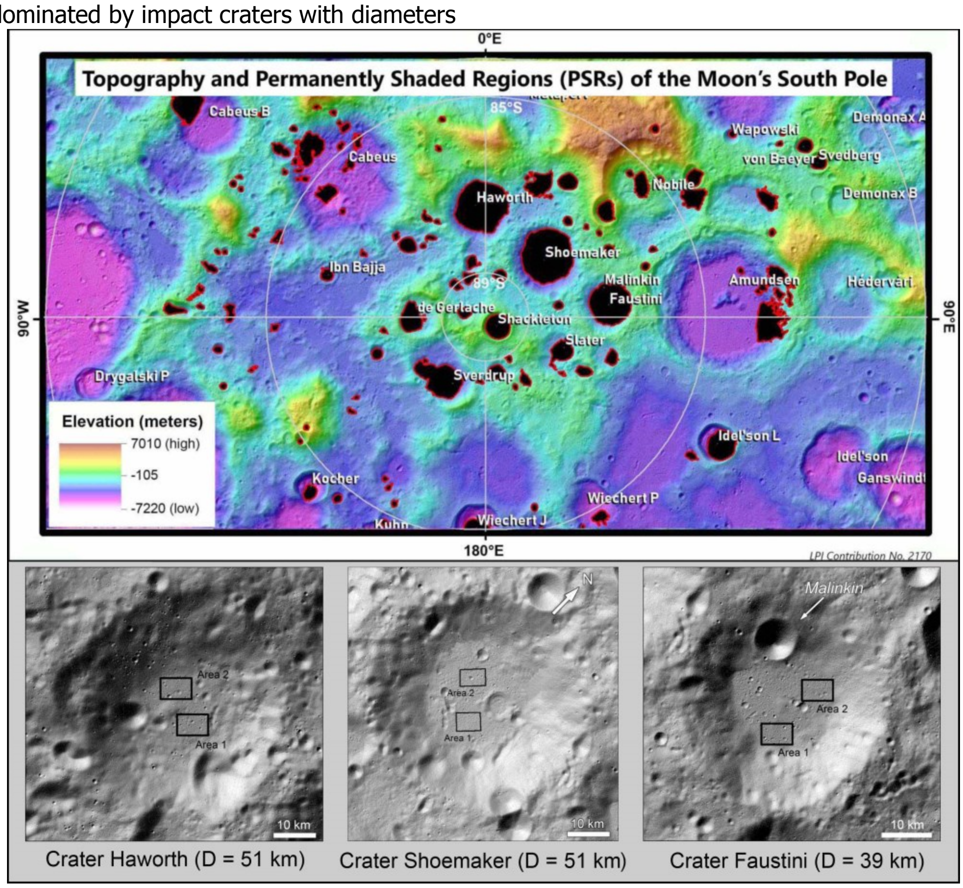


**Figure. 1.** Above: Topographic map of the south-polar region (https://www.lpi.usra.edu/lunar/lunar-so uth-pole-atlas/maps/SPole_80S_LOLA-PSR_v20190515.pdf). In black are shown permanently shadowed areas. Below: The hill-shade images of the studied craters Haworth, Shoemaker and Faustini. Rectangles on their floors show localities of the Study areas.

Authors of this work studied morphology of the surface of the permanently shadowed floor of the south-polar crater Shoemaker and compared it with surface morphology in the normally illuminated by Sun Lunokhod-2 working area and Apollo-16 landing site (Basilevsky and Li, 2024). It was found that in the morphology of the permanently shadowed floor of crater Shoemaker, as well as in that of the illuminated by Sun areas, is dominated by populations of craters with diameters of tens to hundreds of meters. It was also found that craters with diameters of 150 to 400 m in permanently shadowed and in illuminated places have approximately the same depth to diameter ratios. In the present study the analysis of characteristics of floors of two other south-polar craters, - Haworth and Faustini, - is involved and correspondingly the surface characteristics of already three permanently shadowed areas are discussed and compared with those in normally illuminated ones. Images of craters in the lower part of Figure 1 and the Study areas on their floors in Figure 2 were obtained by the hill-shade technique using digital terrain models (DTMs) created from the laser altimeter LOLA data (https://pds-geosciences.wustl.edu/lro/lro-l-lola-3-rdr-v1/lrolol_1xxx/DATA/LOLA_GDR/POLAR/JP2/LDEC_875S_5M.JP2). Images of the study areas in the Lunokhod-2 and Apollo-16 sites were obtained by the same technique, but using DTMs created by stereophotogrammetrical analysis of LROC NAC images (Lunar Reconnaissance Orbiter).

It is seen in Figure 1 that floors of the three considered craters are permanently shadowed. The 4.5 x 6 km Study areas on them are placed on the plain-like approximately horizontal surfaces of these floors outside craters larger than 1 km in diameter and relatively large positive landforms.

Figure 2 shows rather detailed images of the Study areas on the floors of the three considered craters as well as the Study areas in the Lunokhod-2 and Apollo-16 sites. It is seen in these images, that the surface morphology of the permanently shadowed floors of the three considered craters is dominated by populations of craters with diameters of tens to hundreds of meters that is also typical for normally illuminated plains of lunar maria and the lunar highland plains. In all eight Study areas based on spatial density of craters larger 100 m in diameter were estimated model ages of the surface. They are 1.8 ± 0.2 and 2.4 ± 0.2 Ga for the Faustini Study areas, 3.6 ± 0.03 and 3.8 ± 0.03 Ga for the Shoemaker ones and 1.5 ± 0.2 and 1.5 ± 0.2 Ga for the Haworth ones. For the Lunokhpod-2 working area the model age was found to be 2.5 ± 0.1 Ga and for the Apollo-16 site, 3.9 ± 0.02 Ga. These estimates agree with the earlier made datings for the crater Shoemaker floor (Tye et al., 2015), for the Lunokhod working area (Hiesinger et al., 2000) and for the Apollo-16 landing site (Stoffler and Ryder, 2001). For the floors of Faustini and Haworth our estimates are significantly lower than those received by Tye et al. (2015). Probably this is due to the fact that placing our Study areas on the floors of these two craters we avoided craters with diameters larger than one kilometer and in can be seen in Figure 1 that such craters are present there.

For crater with diameters from 150 to 400 m using the mentioned above digital terrain models were measured ratios of crater depth (d) to diameter (D) (Table 1).

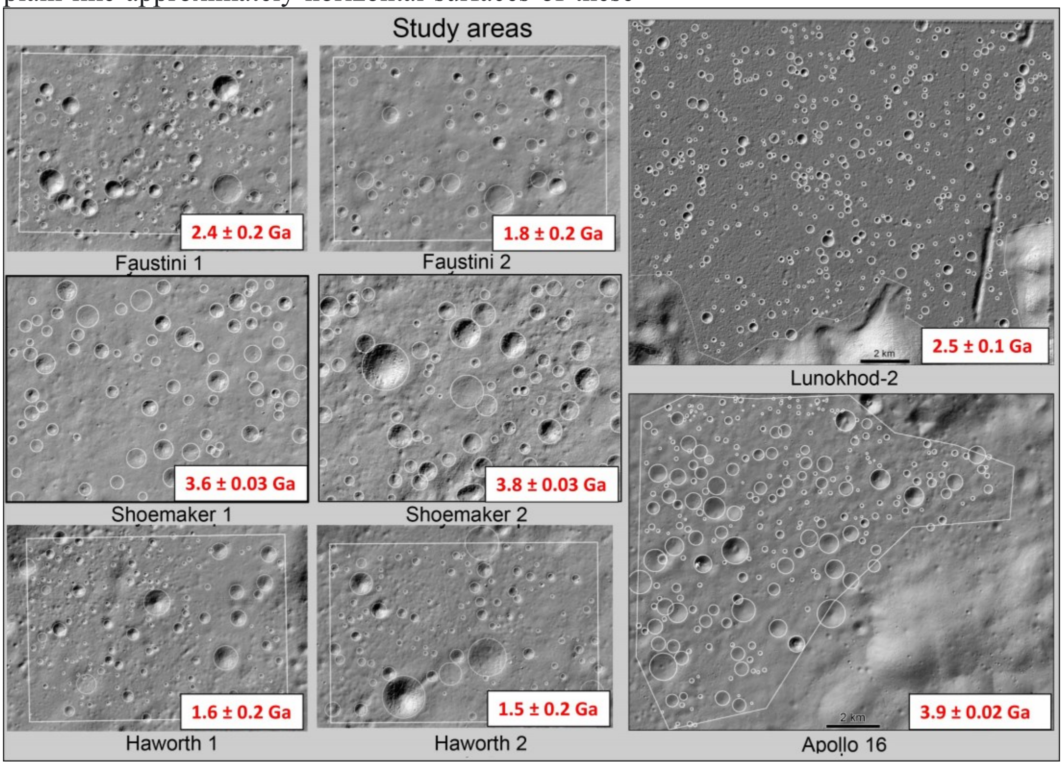


**Figure 2.** The Study areas on the floors of craters Faustini, Shoemaker, Haworth, as well as in the Lunokhod-2 working region and the Apollo-16 landing site. Red digits show the model absolute age (billions of years) estimated from the spatial density of small craters.

**Table 1.** Ratios of crater depth (d) to its dtiameter (D)

| No | Study areas | Number of craters with D = 150-400 m | Mean d/D value | Standard deviation of d/D value |
|---|---|---|---|---|
| **1** | Faustini 1 | 48 | 0.114 | 0.0367 |
| **2** | Faustini 2 | 40 | 0.090 | 0.0321 |
| **3** | Shoemaker 1 | 74 | 0.073 | 0.0226 |
| **4** | Shoemaker 2 | 60 | 0.088 | 0.0289 |
| **5** | Haworth 1 | 44 | 0.118 | 0.0315 |
| **6** | Haworth 2 | 47 | 0.099 | 0.0466 |
| **7** | Lunokhod-2 | 288 | 0.082 | 0.0421 |
| **8** | Apollo-16 | 130 | 0.114 | 0.0360 |

So, analysis of the surface morphology within six 4.5 x 6 km Study areas on the permanently shadowed floors of the south-polar lunar craters Faustini, Shoemaker and Haworth showed that it is rather similar to the morphology in the "normally" illuminated by Sun mare and highland plains within the Lunokhod-2 and Apollo-16 sites and it is dominated by populations of impact craters with diameters of tens to hundreds of meters. The ratios of crater depth to diameter of the craters having diameters from 150 to 400 m within the permanently shadowed areas are about the same as within the "normally" illuminated mare and highland plain areas. These conclusions are important for planning, transportation and work of robotic and piloted rovers in the permanently shadowed regions of the Moon. More detailed information on morphology and some other characteristics of the surface will hopefully be obtained from analysis of images with nominal resolution 1.7 m/px taken by the constructed with NASA USA support ShadowCam camera (https://www.shadowcam.asu.edu/) onboard Korea Pathfinder Lunar Orbiter. To obtain images of the permanently shadowed crater floors will be enough solar light reflected from the illuminated tops of the crater rims.

*Sources of funding: The work was done under the GEOKHI RAS state assignment (A.T. Basilevsky) and supported by Suzhou Vocational University (Yuan Li).*

### References

1. Basilevsky A.T. and Li Yuan. Surface morphology inside the PSR area of lunar polar crater Shoemaker in comparison with that of the sunlit areas. Planetary and Space Science. 2024, V. 241. 105839. 10 p.
2. Colaprete A. and 16 coauthors. Detection of water in the LCROSS ejecta plume. Science. 2010. V. 330. 463–468.
3. Hiesinger H., Jaumann R., Neukum G., Head J.W. Ages of mare basalts on the lunar nearside. J. Geophys. Res. 2000. V. 105 (el2), 29,239-29,275.
4. Stoffler D. and Ryder G. Stratigraphy and isotope ages of lunar geologic units: chronological standard for the inner Solar system. Space Sci. Rev. 2001. V. 96, 9–54.
5. Tye A.R., Fassett, C.I., Head, J.W., Mazarico, E., Basilevsky, A.T., Neumann, G.A., Smith, D.E., Zuber, M.T., 2015. The age of lunar south circumpolar craters Haworth, Shoemaker, Faustini, and Shackleton: implications for regional geology, surface processes, and volatile sequestration. Icarus 255, 70–77.

**Glazovskaya L.I. [1], Piryazev A.A. [2,3]., Shcherbakov V.D. [1]** **Shock transformation of zircon in Logoisk (Belarus) impacties.**

[1]Geological Faculty, Lomonosov Moscow State University, Moscow, Russia, [2] Faculty of Chemistry, Lomonosov Moscow State University, Moscow, Russia ,[3] Institute of Problems of Chemical Physics, Russian Academy of Sciences, Chernogolovka, Russia
Liudmilaglazov@yandex.ru)

**Abstract.** The transformation of zircon in glasses of suevite of the Logoisk structure has been studied. Various types of its transformation have been revealed: the formation of granular textures both in the rims around the zircon grains and in the inner parts of the grains. Some zircon grains are converted into a fully granular aggregate of crystallites. The transition of zircon to reidite- high-density modification of zircon, the formation of planar fractures and the decomposition of zircon into $ZrO_2$ and $SiO_2$ have been established. The rims of the diaplectic and melting glass around the zircon grains were found. The amorphous state of zircon in these rims has been proven by micro Raman spectroscopy. The occurrence of granulated zircon grains with impact melt in the space between its crystallites corresponds to a temperature >2000°C. An assessment of the P-T conditions for the formation of impact glass of suevite according to the conditions of zircon transformation was carried out.

***Keywords**: impactites, zircon, reidite, diplectic and fused glasses of zircon.*

The 17 km diameter, 30 ± 5 Ma old Logoisk structure in Belarus was intensively drilled within the crater area (29 boreholes). The age of the structure was determined by the $^{40}Ar/^{39}Ar$ method. The Logoisk impact structure consists of a two-layer basement: Archean granite gneiss and Late Proterozoic and Middle Devonian horizontally layered sedimentary rocks (the thickness of the sedimentary rocks 200- 300 m). The upper part of the structure comprised of Paleogene–Neogene lacustrine sediments (27–291 m thick) and 102–324 m of thick Quaternary sedimentary rocks. Granite gneiss experienced shock metamorphism to a depth of 150 meters. Currently, the Logoisk impact structure is the most drilled on Earth.

Zircon is the most informative mineral for determining the PT conditions of impactite formation, since its transformation occurs in a wide range of temperatures and pressures from temperatures of 500°C to 2376°C (corresponds to the formation of ZrO2 cubic syngony). The transformation of zircon in Logoisk structure impactites includes the formation of granular textures, the transition of zircon to reidite, a high-density modification of zircon, which is proved by the method of micro-Raman spectroscopy.

The formation of planar fractures in zircon is observed in two directions. The decomposition of zircon into $ZrO_2$ and $SiO_2$. may be accompanied by the removal of $SiO_2$ into the impact melt. The degree of impact can vary from grain to grain.

**Methods.** Raman spectra were acquired on a Horiba LabRam Evolution Raman spectrometer, equipped with a laser wavelength of 633 nm, using a laser power of 17 mW. The spectrometer is equipped with two diffraction gratings, a high-performance detector cooled by a Peltier element, and a set of neutral gray filters to adjust the radiation power on the sample. The optical microscope has a resolution of 500 nm. The measurements were carried out with a grating of 1800 lines per mm, the laser power was 25% of the maximum, and the objective was ×100. The exposure time was 10 s with two accumulations.

**Reidite.** Reidite is currently documented in several terrestrial impact structures: Ries, Germany; Haughton, Canada; Xiuyan, China; Chicxulub, Mexico; Woodleigh, Australia; Rock Elm, United States; Chesapeake Bay, United States; Reidite was discovered in shocked zircon from the Stac Fada impactite, Scotland and in the Rochechouart impact structure, France. Reidite has been identified in the HED meteorite NWA 2650 and lunar meteorite SaU 169.

Reidite was proved by micro-Raman spectroscopy in the impact rocks of the Logoisk impact structure (Glazovskaya et al., 2024). The EBSD mapping method made it possible to prove the presence of "former reidite" in the suevite of the Logoisk structure, that is, reidite, which at temperatures exceeding 1100°C passed back into zircon. Zircon can completely transform into reidite or partially. The presence of reidite in the zircon grain suggests a pressure of 17.5 – 53 Gpa (Erickson et al., 2020).

**Planar fractures.** Planar fractures in two directions are described by us in a thin section of suevite glass, in a thin crack of impact glass in biotite. In the same zircon grain, reidite is present, proven by the method of micro-Raman spectroscopy and the region of decomposition of zircon into $ZrO_2$ and $SiO_2$. $ZrO_2$ is present both in the form of a border around a part of the grain and in the form of the thinnest separations sprayed in the central part of the grain. These areas are diagnosed by the ratio of $ZrO_2$ and $SiO_2$ in the zircon structure, which becomes 1.30- 1.34. The presence of planar fractures together with the absence of reidite makes it possible to estimate the pressure as 20-40 GPa. In this grain, the simultaneous presence of planar fractures, reidite (stable up to T -1200 °C), a baddeleyite rim and signs of zircon decomposition into $ZrO_2$ and $SiO_2$ (T exceeding 1676 ° C) indicates an uneven distribution of pressure and temperature in this grain on a microscopic scale.

**Granular textures**. Granular textures in zircon made of glass of the Logoisk impact structure are associated with microscopic inclusions of $ZrO_2$ formed as a result of dissociation of zircon into $ZrO_2$ and $SiO_2$; silica is often carried out into the surrounding melt. Granular textures are installed both in the borders (Fig. 1) around the zircon grains and in the inner parts of the grains. In the inner parts of the grains, in the intervals between the crystallites, there is a zircon-type diplect glass. The presence of $ZrO_2$ in the granular zircon (Figures 1) of the Logoisk structure suggests an impact pressure of 65–70 GPa and postshock temperatures higher than 1675°C.

The presence of fully granular zircon grains with an impact melt in space between the crystallites in the impactites of the Logoisk structure makes it possible to estimate the temperature of the impact melt as exceeding 2000°C, in accordance with the diagram (Timms et al., 2017).

**Zircon amorphization.** Zircon amorphization can occur at the solid-phase stage with the formation of a diplectic glass. Previously, diplect glass in zircon was described only in association with reidite (Meteor crater), while its presence was not proven by instrumental methods. Amorphous areas in the zircon grain may also be the result of melting zircon.

We have obtained petrological evidence of the melting of zircon in the suevite of the Logoisk structure. Prior to this, only indirect petrological evidence of zircon melting in natural impactites was known: crystallization of baddeleyite from an impact melt (Boltyshsky crater, Gurov et al., 2015), finding zircon domains that do not correspond in orientation to crystalline zircon and reidite (EBSD mapping method for zircon from impactites of the Vredefort structure, South Africa) (Kovaleva et al., 2021). Zircon amorphization was achieved in experiments at a pressure of 60 GPa to the complete absence of spectral bands of Raman spectroscopy in the peripheral parts and rims (Gucsik et al., 2002).

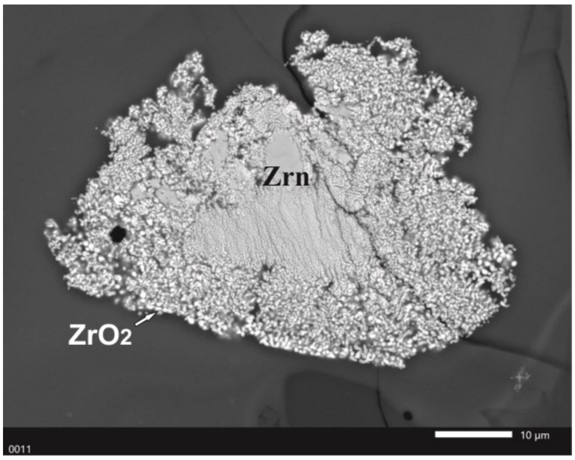


**Fig. 1** Rim of granular textures in zircon with dissociation of zircon into $ZrO_2$ and $SiO_2$

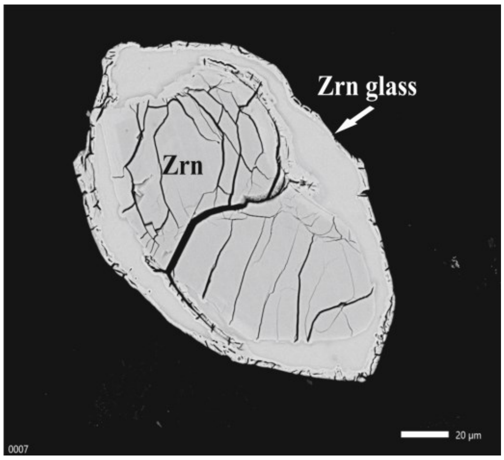


**Fig. 2**. Rim of fused zircon glass from the suevite of the Logoisk structure

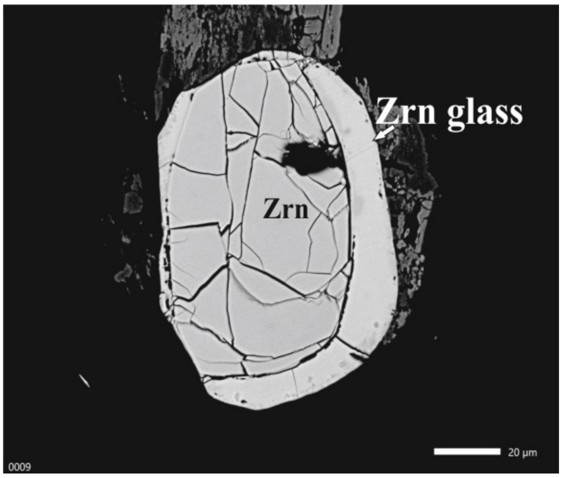


**Fig 3.** Rim of zircon diaplectic glass from suevite of the Logoisk structure

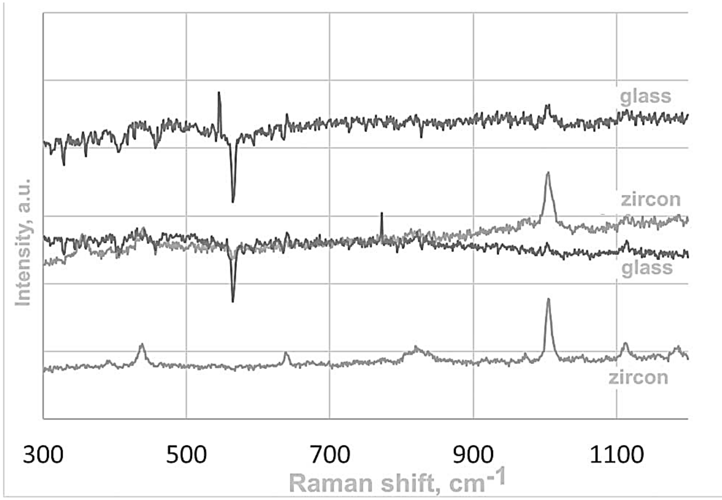


**Fig. 4.** Raman spectroscopy in zircon (grey lines) and diaplectic glass (dark lines) from Logoisk structure.

Diaplectic and fused glasses in the rims of zircon from the matrix of suevite of the Logoisk impact structure, shown in the figure 2, 3. Their presence was proved by micro-Raman spectroscopy (Fig. 4). The amorphization of zircon in the form of diaplectic glass was also found and confirmed by micro-Raman spectroscopy in impact zircon from the stratified Yarva-Varaka massif (Kola Peninsula) (Kaulina et al., 2017).

Diaplectic glasses are a product of amorphization at the solid-phase stage , the substance is crushed by a shock wave into tiny (<100 Å) fragments (Feldman, Glazovskaya, 2018) that are not identified as a crystalline material by X-ray diffraction.

Diplectic glasses are formed while preserving the boundaries of minerals. In the Logoisk structure, diplectic transformations are also observed for quartz, plagioclase, and kalishpate. When the rims of the diplectic glass are formed, the inner parts of the zircon grains are shielded by the rim and retain their structure.

An amorphous phase of the zircon composition was described in experimental samples at impact pressures of 40 GPa in the form of plates in zircon grains containing planar fractures (PDFs), a partial transformation to reidite was observed in the same grains. While at higher experimental pressure (60 GPa), complete transformation to reidite was observed in experiments.

**Conclusion**. Upon impact on the target rocks of the Logoisk structure, zircon undergoes transformations (granular textures, transition to reidite - a high-density modification of zircon, formation of planar fractures, decomposition of zircon into $ZrO_2$ and $SiO_2$, amorphization at the solid-phase stage with the formation of diplectic and fused glass. The transformations of zircon takes place in the temperature range from the first hundred degrees to temperatures exceeding 2000°C.

**References**

Glazovskaya, L. I., Parfenova, O. V., and Ilkevich, G. I. 1993. Impactites of Logoisk Astrobleme. Petrology 1: 834–844 (in Russian).

Kaulina T.V., Nerovich L.I., Bocharov V.I., Lyalina L.M., Ilchenko V.L., Kunakkuzin E.L., Kasatkin I.A. 2017. Raman spectroscopy of impact zircon from a layered Yarva-Varak body. (Monchegorsky ore district, Kola Peninsula) Bulletin of the Moscow State Technical University. Vol. 20, No. 1/1. pp. 72-82.

Feldman, V. I., and Glazovskaya, L. I. 2018. Impactgenez KDU, 151 p (in Russian).

Glazovskaya L.I., Shcherbakov V.D., Piryazev A.A. **2024**, Logoisk impact structure, Belarus: Shock transformation of zircon, *Meteoritics and Planetary Science*, v. 59, № 1, p. 88-104

Gucsik A., Koeberl C., Brandsta«tter B, Reimold W.U, Libowitzky E. 2002. Cathodoluminescence, electron microscopy, and Raman spectroscopy of experimentally shock-metamorphosed zircon. Earth and Planetary Science Letters 202. p 495-509.

Gurov, E. P., Shekhunova, S. B., and Permyakov, V. V. 2015. Accessory and Opaque Minerals in Impact Melt Rocks of the Boltysh Structure, Ukraine. Meteoritics & Planetary Science 50: 1139–55.

Erickson, T. M., Cline, C. J., Jakubek, R., Cintala, M. J., and Timms, N. E. 2020. Shock Deformation in Zircon, a Comparison of Results from Shock-Reverberation and Single-Shock Experiments. 51st Lunar and Planetary Science Conference, abstract # 1581.

Kovaleva, E., Kusiak, M. A., Kenny, G. G., Whitehouse, M. J., Habler, C., Schreiber, A., and Wirth, R. 2021. Nano-Scale Investigation of Granular Neoblastic Zircon, Vredefort Impact Structure, South Africa: Evidence for Complete Shock Melting. Earth and Planetary Science Letters 565: 116948.

Masaitis, V. L. 1999. Impact Structures of Northeastern Eurasia: The Territories of Russia and Adjacent Countries. Meteoritics & Planetary Science 34: 691–711.

Timms, N. E., Erickson, T. M., Cavosie, A. J., Reddy, S. M.,Nemchin, A. A., Schmieder, M., Pearce, M. A., Tohver, E., Zanetti, M. R., and Wittmann, A. 2017. A Pressure-Temperature Phase Diagram for Zircon at Extreme Conditions. Earth-Science Reviews 165: 185–202.

## Gorbachev P.N., Bezmen N.I. First results of experimental Modeling of the chondritic structure of meteorites. *UDC 550.4*

Korzhinskii Institute of Experimental Mineralogy RAS Chernogolovka, Chernogolovka, Moscow district, Russia: p_gor@mail.ru

**Abstract.** A chondrites are a type of stony meteorites, characterized by the presence of chondrules - oval-shaped crystallized silicate precipitates in a Fe-sulfide-metallic matrix. The conditions for the formation of chondrules are still the subject of the discussion. The experiments were carried out for modeling the chondrite structure in a high gas pressure equipment at T = 1000ºC and a pressure of 1 kbar using a model composition corresponding to C3 carbonaceous chondrites.

***Keywords**: chondrite, experiment, modeling, chondrules, matrix*

**Experimental technique.** The experiments were run in the the internally heated gas media pressure vessel. As a starting composition, we used a model mixture whose composition corresponded to the anhydrous composition of the Orgail meteorite. The mixture in powder form was pressed into a graphite capsule (15 mm long, 6 mm in diameter). The capsule was placed in a Pt-capsules 60 mm long and Ø 7 mm, then water and paraffin were added. The experiment temperature was 1000ºC, P = 1 kbar, $X\mathrm{H_2}$ = 0.3, duration was 24 hours. After the experiment, a graphite capsule was removed from the Pt-capsules and pressed into place. Fig. 1 shows a quenching sample after the experiment. Then the sample was studied using optical methods and a microprobe.

**Results and discussion.** The results of the experiment are in table. 1 and in Fig. 2.

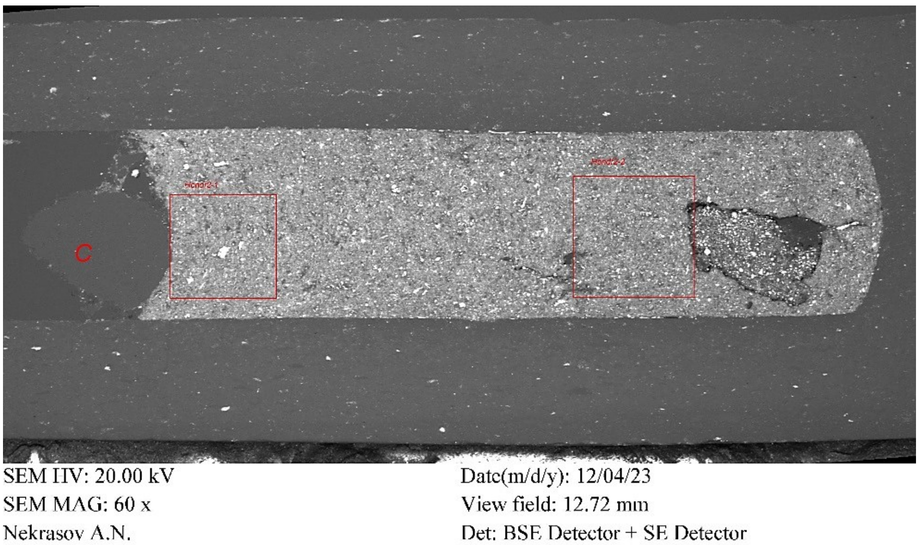


**Fig. 1.** Quenching sample after the experiment.

**Table 1.** Comparison of the composition (wt.%) of the Orgail carbonaceous chondrite with the general matrix composition of the sample obtained during the experiment.

| | Orgail | Experiment* | Matrix** | Chondrule*** |
|---|---|---|---|---|
| $Na_2O$ | 0.8 | 0.71 | 0.88 | 2.26 |
| MgO | 17.01 | 23.22 | 27.05 | 14.36 |
| $Al_2O_3$ | 1.78 | 2.76 | 3.1 | 10.25 |
| $SiO_2$ | 24.28 | 30.74 | 36.79 | 62.09 |
| $K_2O$ | 0.08 | 0.07 | 0.09 | 0.54 |
| CaO | 1.31 | 1.13 | 1.34 | 6.22 |
| $H_2O$ | 21.41 | | 0.48 | 1.58 |
| MnO | 0.2 | 0.58 | 0.22 | 0.31 |
| FeO | 12.26 | 29.73 | 23.2 | 1.28 |
| FeS | 16.22 | | | |
| NiO | 1.32 | 1.22 | 0.99 | 0.06 |
| C | 3.34 | | | |
| Total | 100 | 100 | 100 | 100 |

Note:
Orgail carbonaceous chondrite (Voitkevich et al, 1990),
* average composition of the quenched sample obtained in the experiment,
** average composition of the matrix of the quenched sample,
*** average composition of oval-shaped microinclusions (chondrules).

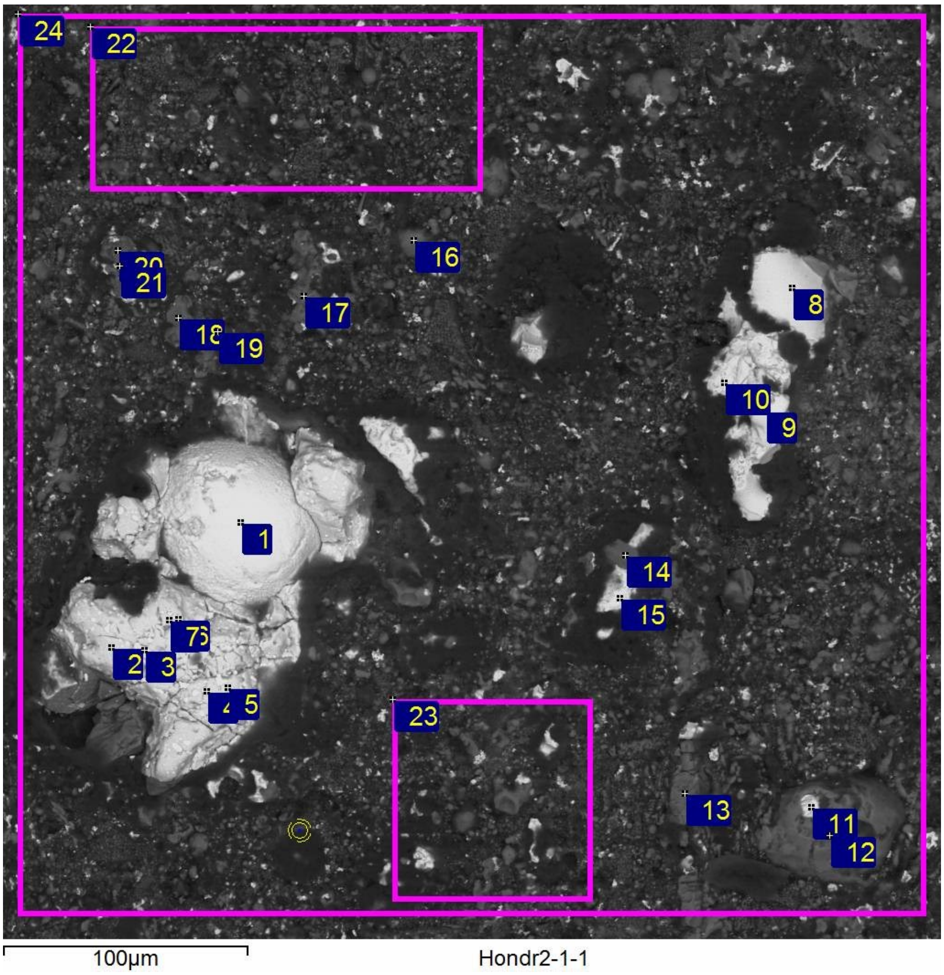


**Fig. 2.** Microphotograph of a section of a quenched sample with analyses.

The quenched sample, the chemical composition of which is close to the composition of the original mixture, has a crystalline, unevenly granular structure, similar in chemical and phase composition to carbonaceous chondrites (see table 1).

The matrix (analysis areas 22, 23) is characterized by a microgranular texture, ultra-basic composition, with a high content of magnesium (up to 27 wt.% MgO), iron (up to 23 wt.% FeO) with inclusions of silicate, Fe-metallic and Fe-sulfide phases.

The silicate fraction is represented by oval-shaped microinclusions (chondrules) up to 10 microns in size, the composition close to magnesian basalt, forsterite of olivine and enstatite orthopyroxene composition.

The ore fraction consists of intergrowths of metal phases, almost pure Fe, Fe-Ni alloy with variable Fe and Ni content (from 5-6 to 16-20 wt.% Ni), as well as troilite.

Features of the texture, chemical and phase composition of the quenched samples indicate that recrystallization of the starting mixture during the experiment led to the formation of carbonaceous chondrites.

*This study is fulfilled under Research program № FMUF 2022-0004 of the Korzhinski Institute of Experimental Mineralogy.*

**Reference:**

Voitkevich G.V., et.al. Handbook of geochemistry. - Moscow. Nedra. - 1990.

## Guseva E.N. and Ivanov M.A. Spatial-genetic relationships corona-sources of volcanism and volcanoes of Venus. *UDC 523.42*

Vernadsky institute of RAS, 119991, Moscow, Russia, guseva@geokhi.ru, ivanov.m@geokhi.ru

**Abstract** We analyzed the spatial-genetic relationships of the coronae that are sources of the younger lobate plains and the volcanoes of Venus and have found that: coronae representing the sources of lobate plains, as well as large flattened and medium-sized conical volcanoes, are distributed on the surface mainly in the Beta-Atla-Themis, Eistla and Metis regions; the dome-like corona sources of lobate plains and large flattened volcanoes are often spatially related to each other. It is likely that these volcanoes represent transitional landforms from coronae to volcanoes. The studied coronae and volcanoes mark the main areas of the late volcanic activity on Venus.

***Keywords**: Venus, landforms, coronae, volcanoes, lobate plains, late volcanism.*

We analyzed characteristics of the spatial distribution of coronae - large (with a diameter of up to 2500 km) circular features (Stofan et al., 1992; Crumpler, Aubele, 2000), which probably represent the surface manifestations of mantle diapirs (Nikishin, 1990; Pronin, Stofan, 1990; Stofan, Smrekar, 2005), and volcanoes, the topographically prominent centers of volcanism (Head et al., 1992; Crumpler et al., 1997). Both these types of features are sources of flows of lobate plains (pl) that represent the youngest manifestations of volcanic activity on the planet (Ivanov, Head, 2013; Hahn, Byrne, 2023).

The coronae, which are the sources of lobate plains, compose about 17% of the entire population of coronae and are characterized by three topographic classes: D, W, U (domes, depressions with a central peak, simple depressions, Fig. 1) (Guseva, Ivanov, 2023). These classes probably correspond to the different stages of evolution of coronae (Smrekar, Stofan, 1997).

Volcanoes are characterized by three size groups: the largest flat-topped (up to 740 km in diameter), medium conical (up to 425 km) and small conical (up to 240 km) (Fig. 2).

The purpose of the study was to determine the main areas of concentration of the studied structures on the surface of Venus and to establish their possible genetic relationships.

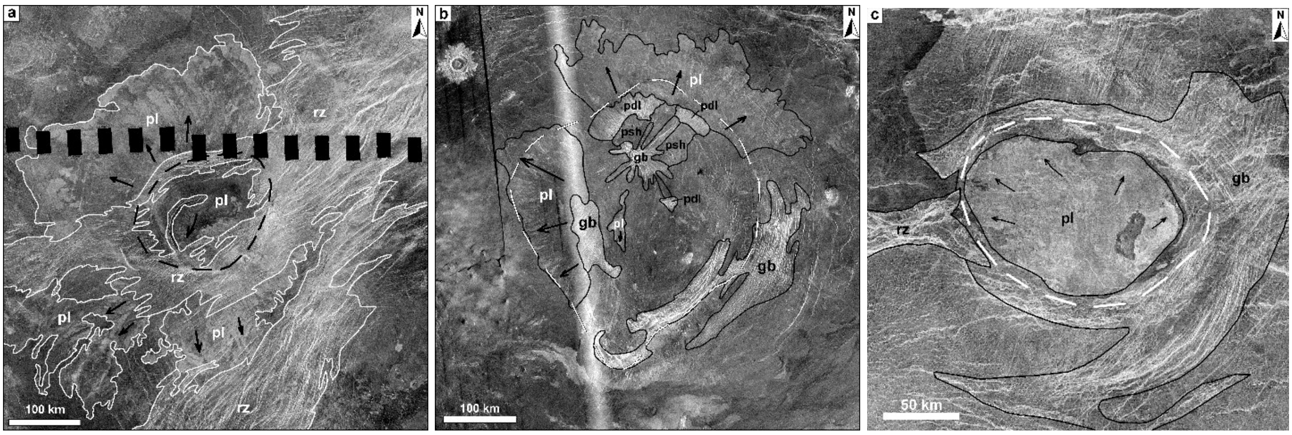


**Figure 1.** Coronae sources of lobate plains (pl) of three topographic classes: a – Nahas-tsan Mons, class D, 14°N, 205°E, d=167 km; b – Ereshkigal, class W, 21°N, 84°E, d=334 km; c – Rind, class U, 8°N., 247°E, d=137 km.

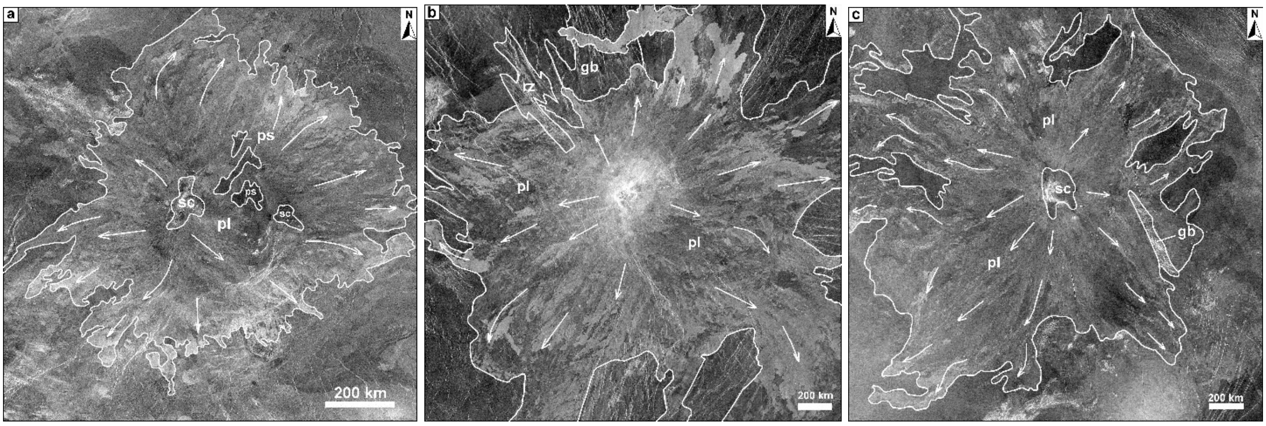


**Figure 2.** Volcanoes of three topographic groups with flows of lobate plains (pl): a – Kokyanwuti Mons, group 1, 36°N, 211°E, d=464 km; b – Idunn Mons, group 2, 47°S, 215°E, d=306 km. c – Xochiquetzal Mons, group 3, 3.5°N, 270°E, d=204 km.

We studied the morphology of the coronae and volcanoes of Venus visible in the mosaics of the C1-MIDR images (resolution ~ 225 m/px) (Figs. 1 and 2), constructed a series of topographic profiles through these structures using the Magellan topographic map (resolution ~ 5 km/px) (Fig. 3), and assessed their stratigraphic position using the geological map of Venus (Ivanov, Head, 2011).

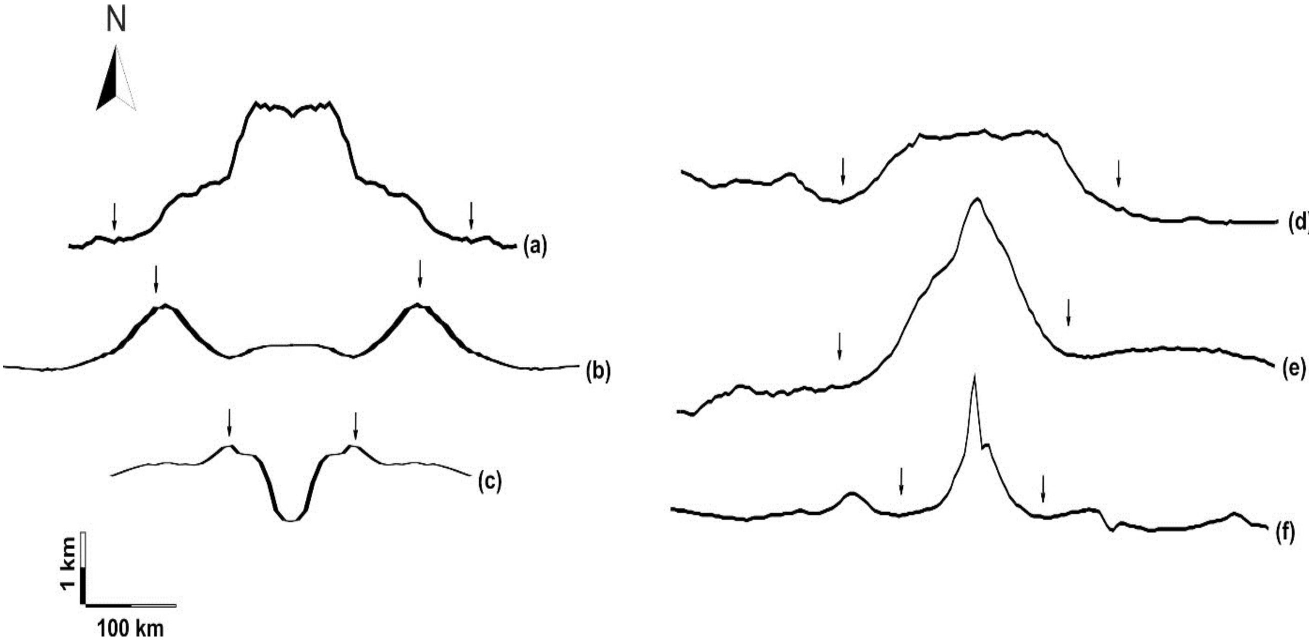


**Figure 3.** Topographic profiles, left: coronae, the sources of lobate plains, a – Nahas-tsan Mons, class D; b – Ereshkigal, class W; c – Rind, class U; right: volcanoes: d – Kokyanwuti Mons, group 1; e – Idunn Mons, group 2; f – Xochiquetzal Mons, group 3.

We have identified the main areas of mutual distribution of the corona-sources of lobate plains (90 structures) and volcanoes (89 structures). The corona-sources of all topographic classes and volcanoes, mainly the large flat-topped (group 1) and medium conical (group 2) (total 53% of the entire population), are concentrated in the BAT (Beta-Atla-Themis), Eistla and Metis regions (Fig. 4). Small conical volcanoes (group 3, 47% of the total population) have a broader distribution over the surface (Fig. 4).

The dome-shaped corona-sources (class D, 44%) and large flat-topped volcanoes (group 1, 27%) are most often spatially associated with each other and are also associated with rift zones in the BAT region (Fig. 5). It is possible that such volcanoes represent advanced stages of the coronae evolution and their transition to more cone-shaped volcanoes.

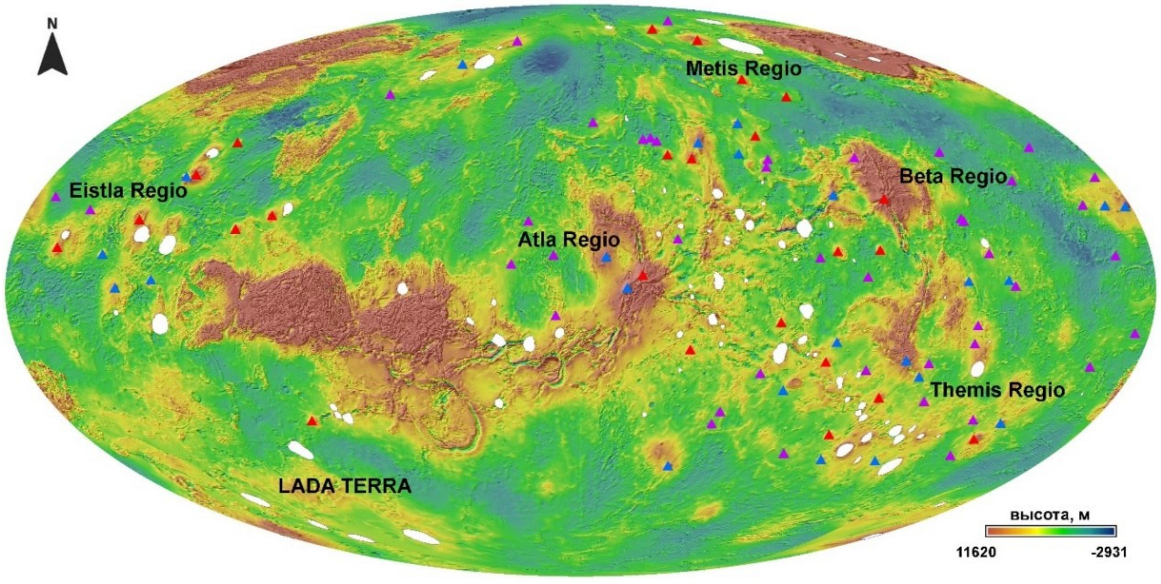


**Figure 4.** The distribution of the corona-sources of lobate plains of three topo-classes (white) and volcanoes of three groups: large flat-topped (group 1, red), medium conical (group 2, blue) and small conical (group 3, purple). The base topographic map: Mollweide projection, central meridian is 180°.

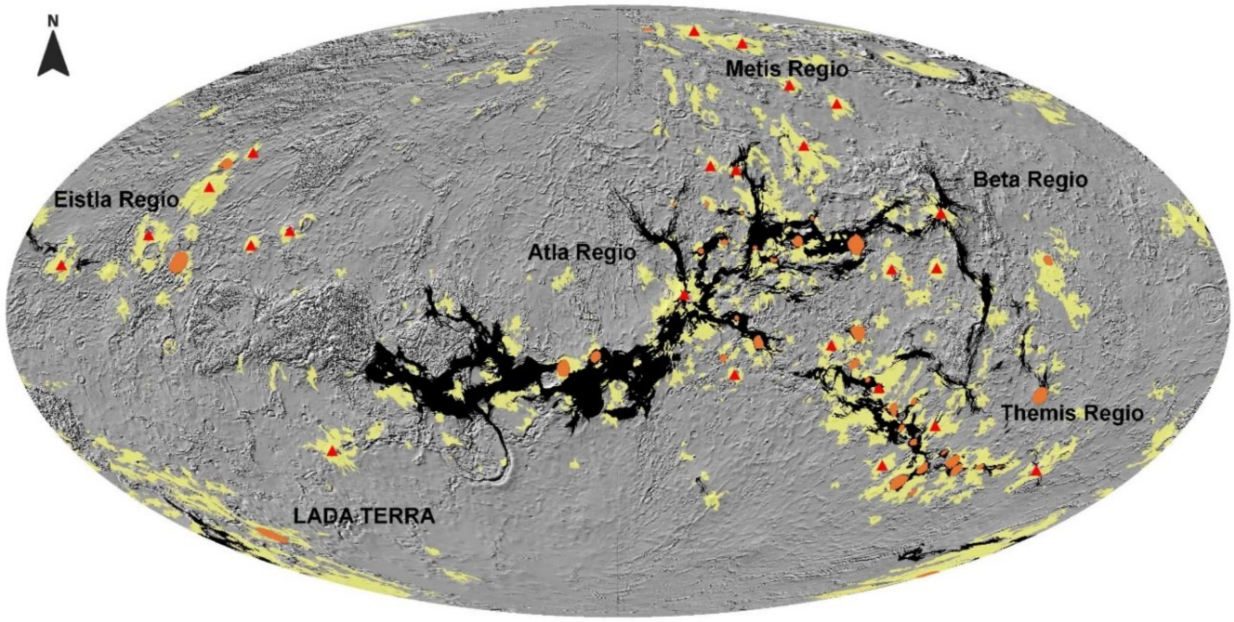


**Figure 5.** The spatial distribution of the dome-shaped corona-sources (D class, orange) and the large flat-topped volcanoes (group 1, red); lobate plains are yellow, rift zones are black; geological boundaries according to (Ivanov, Head, 2011); Mollweide projection, central meridian 180°**.**

Based on the results of our work, we can draw the following conclusions: (1) corona-sources of lobate plains, the large flat-topped and medium-conical volcanoes occur mainly in three areas, the BAT (Beta-Atla-Themis), Eistla, and Metis; (2) the dome-shaped corona-sources and large flat-topped volcanoes are often spatially associated with each other and such volcanoes are likely the result of advanced evolution of coronae; (3) the studied features mark the main areas of late volcanism on Venus.

*The study was carried out under the State Assignment of the Vernadsky Institute of Geochemistry and Analytical Chemistry of the Russian Academy of Sciences.*

**References**

1 Crumpler L.S., Aubele J. Volcanism on Venus, in Encyclopedia of Volcanoes, Houghton B., Rymer H., Stix J., McNutt S., Sigurdson H., Eds., San Diego: Acad. Press. 2000. 727-770.

2 Crumpler L. S., Aubele J. C., Senske D. A., Keddie S. T., Magee K. P., Head J. W. Volcanoes and centers of volcanism on Venus. In Bougher S.W., Hunten D. M., Philips R. J. (Eds.), Venus II: Geology, geophysics, atmosphere, and solar wind environment. The University of Arizona Press. 1997. 697–756.
3 Guseva E.N., Ivanov M.A. Spatial and genetic relationships of coronae, lobate plains and rift zones of Venus. Sol. Syst. Res. 2023. V. 57 (2). 112-121.
4 Hahn R.M., Byrne P.K. A Morphological and Spatial Analysis of Volcanoes on Venus. J. Geophys. Res. 2023. 128. e2023JE007753.
5 Head J.W., Crumpler L.S., Aubele J.C., Guest J., Saunders R.S. Venus volcanism: Classification of volcanic features and structures, associations, and global distribution from Magellan data, J. Geophys. Res., 1992. V. 97. 13.153-13.197.
6 Ivanov M.A., Head J.W. Global geological map of Venus. Planet. Space Sci. 2011. V. 59. 1559-1600.
7 Ivanov M.A., Head J.W. The history of volcanism on Venus. Planet. Space Sci. 2013. V. 84. 66-92.
8 Nikishin A.M. Tectonics of Venus: A review, Earth, Moon, and Planets. 1990. V. 50/51. 101-125.
9 Pronin A.A., Stofan E.R. Coronae on Venus: Morphology and distribution. Icarus. 1990. V. 87. 452-474.
10 Smrekar S. E., Stofan E. R. Corona formation and heat loss on Venus by coupled upwelling and delamination. Science. 1997. V. 277. 1289-1294.
11 Stofan E.R., Smrekar S.E. Large topographic rises, coronae, large flow field, and large volcanoes on Venus: Evidence for mantle plumes? Geol. Soc. Am. Spec. Pap. 2005. V. 388. 841-861.
12 Stofan E.R., Sharpton V.L., Schubert G., Baer G., Bindschadler D.L., Janes D.M., Squyres S.W. Global distribution and characteristics of coronae and related features on Venus: Implications for origin and relation to mantle processes. J. Geophys. Res. 1992. V. 97 (E8). 13.347-13.378.

**Malyshev D.G.[1], Ernst R.E.[2], Ivanov M.A.[1]**

## Geological history of Samodiva Mons on Venus

[1] Vernadsky Institute RAS, Moscow, Russia (malyshev@geokhi.ru); [2] Carleton University, Ottawa, Canada

**Abstract** Studying the mechanisms of internal heat loss on different planets is an important task for understanding the evolution of the planets of the Solar system. Due to the lack of plate tectonics, the leading mechanism on Venus is intraplate volcanism, one of the typical representatives of which is the volcano Samodiva Mons (13.6° N, 69.0° W). Here the geological structure and history of the volcano are described. As a result of mapping on a scale of 1:500,000, the following morphostructural units (subdivisions) were identified: highly tectonized areas, lava flows, edifice of the volcano, graben systems. Based on geological mapping and analysis of relative ages, three main stages of the formation of the studied area were identified: early tectonic, middle volcanic and late, associated with the tectonic activity of the Samodiva Mons volcano.

***Keywords**: Venus, planetary geology, comparative planetology, Samodiva Mons, lava flows, geological hstory*

**Introduction**: The Samodiva Mons volcano (13.6° N, 69.0° W) and the surrounding area are located to the SE of Beta Regio (Basilevsky, Head, 2007). The interest in studying this volcano is explained by the fact that its activity corresponds to the transition from a global volcanic to a global volcanotectonic regime of resurfacing on Venus (Ivanov, Head, 2015). In addition, the soviet "Venera-10" mission landed near the volcano (16° N, 69° W; ~150 km north of the volcano's summit) (Surkov, 1985).

Geological mapping of the area surrounding the Samodiva volcano (Fig. 1) on a scale of 1:500,000 has not been carried out before. The map presented in our work (Fig. 2) is based on a photogeological analysis of radar images obtained by the Magellan spacecraft (spatial resolution of 100-200 m/pix) (Saunders et al., 1992). This map documents new details important for studying the history of the volcano's formation. Earlier, smaller-scale maps were derived (Grosfils, Head, 1996; Abdrakhimov, Basilevsky, 2002), but the volcanic center of Samodiva Mons was not the main purpose of these studies.

Distinguished morphostructural complexes: highly tectonized areas include tessera and densely lineated plains. The surface of the former has a high radar brightness (increased roughness in the meter-decameter range), consists of at least two sets of intersecting ridges and fractures (10-20 km in length). Densely lineated plains have increased radar brightness, their surface is cross-cut by numerous densely packed straight or curved lineaments (Ivanov, Head, 2015). Massifs of tectonized areas are observed mainly in the north of the studied area and make up the southern tip of the Hyndla Regio.

Most of the study area is covered with lava sheets and flows, which were divided into several subgroups according to morphology, link to different sources, and position relative to the summit of the Samodiva Mons volcano. The flows are represented by lobate (higher radar albedo, clear boundaries, small area) and sheet flows (lower radar albedo, fuzzy/diffuse boundaries and occupy a large area). Possible sources of flows are the Samodiva Mons volcano, small shield volcanoes, Zhivana Corona, Unnamed Coronae to the SE and NE of Samodiva Mons. The sources of sheet flows are usually indistinguishable (Ivanov, Head, 2011).

Samodiva Mons volcano is a shield volcano with a diameter of 150 km, in the upper part there is a depression with a diameter of 25 km and a depth of up to 500 m, as well as a bright dome-shaped formation with a clearly defined frontal ledge. These may be the results of late volcanic activity: a caldera and a dome. The frontal ledge of the dome indicates a higher viscosity of the lavas, for example, due to a more evolved acidic composition (Ivanov, Head, 1999).

Graben systems are assembled into radial and circumferential swarms, spreading mainly from the Samodiva Mons volcano. The summit of the volcano is intersected in a north-south direction by a system of densely packed grabens and fissures extending 145 km north and 223 km south from the top of the volcano. In many cases, graben systems on Venus form over dikes (Buchan, Ernst, 2021), which is confirmed by observations of lava flows flowing from grabens or volcanic structures located on top of a graben.

The relative age estimation is based on the principle of superposition, cross-cutting and embayment relationships (Wilhelms, 1990). In the geological history of the study area, three main stages can be distinguished: early tectonic, middle volcanic and late, associated with the tectonic activity of the Samodiva Mons volcano. During the first stage, tesserae and densely lineated plains were formed. The second stage is the stage of lava flooding, when most of the sheets poured out. The third is the intrusion of dikes and the formation of graben systems, the phase of localized volcanism, when lobate flows were formed.

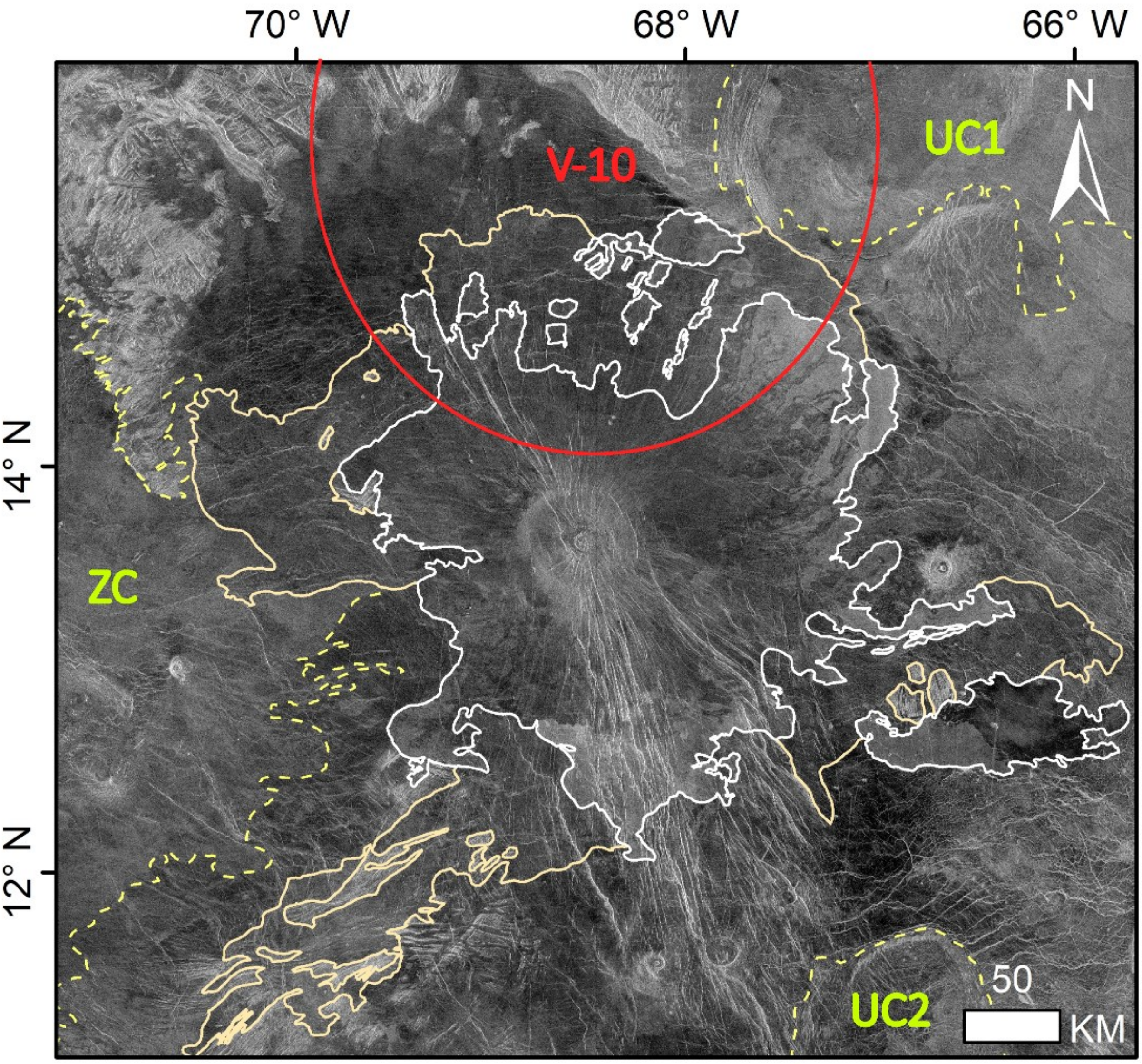


**Figure 1.** Radar image of the study area ~520×561 km (11°-16°N, 66°-71°W), Samodiva Mons is located at the center; *ZC* – Zhivana Corona; *UC1* – Unnamed Corona to the NE; *UC2* – Unnamed Corona to the SE. White solid line indicate the boundary of Samodiva Mons youngest volcanis material (stage 3); yellow solid line – boundary of older Samodiva Mons flows (stage 2); dashed lines – coronae material boundaries; red – «Venera-10» landing site ellipse

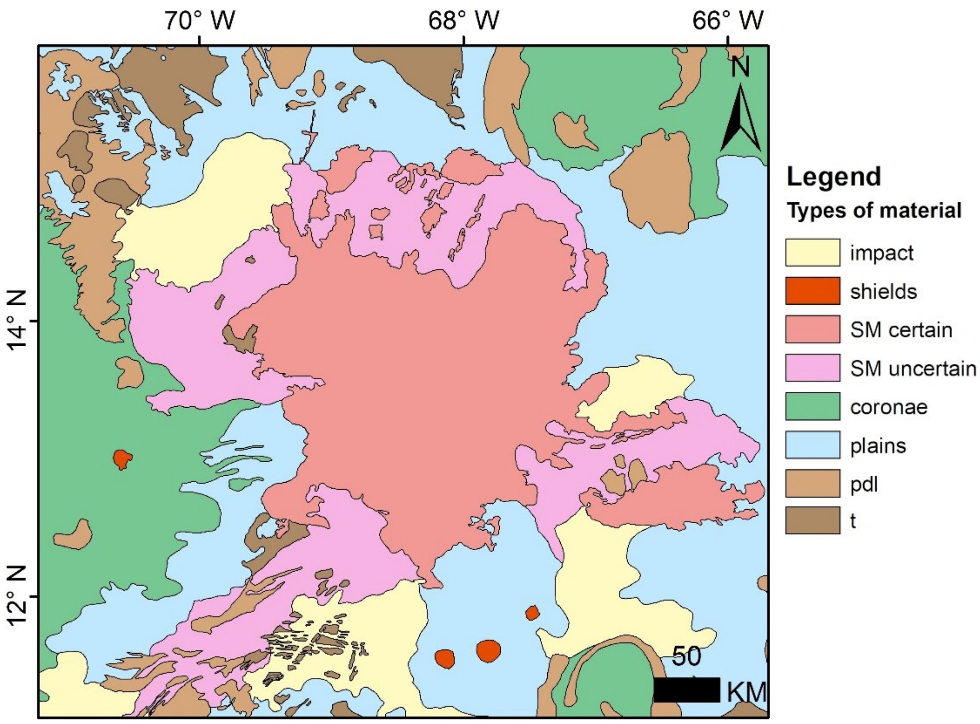


**Figure 2** – Simplified geological map of the study area (1:500,000). Legend: *tt* and *pdl* – tesserae and densely lineated plains (early tectonic stage); *plains*, *coronae*, *SM uncertain* – material of lava plains, coronae and older Samodiva Mons material (stage of lava flooding); *SM certain*, *shields*, *impact* – young material of the volcano Samodiva Mons, small shield volcanoes, impact crater material (the third stage of the studiy area formation)

*Funding: The study was carried out under the State Assignment of the Vernadsky Institute of Geochemistry and Analytical Chemistry of the Russian Academy of Sciences*

**References**

1 Basilevsky A.T., Head J.W. Beta Regio, Venus: Evidence for uplift, rifting, and volcanism due to a mantle plume // Icarus. 2007. V. 192. P. 167–186.
2 Ivanov M.A., Head J.W. The history of tectonism on Venus: A stratigraphic analysis // Planetary and Space Science. 2015. V. 113-114. P. 10–32.
3 Surkov Y.A. Cosmochemical studies of planets and satellites. M.: Science, 1985. 307 p.
4 Saunders R.S., Spear A.J., Allin P.C. [et al.]. Magellan mission summary // J. Geophys. Res. 1992. V. 97, № E8. P. 13067–13090.
5 Grosfils E.B., Head J.W. The timing of giant radiating dike swarm emplacement on Venus: Implications for resurfacing of the planet and its subsequent evolution // J. Geophys. Res. 1996. Vol. 101, № E2. P. 4645–4656.
6 Abdrakhimov A.M., Basilevsky A.T. Geology of the Venera and Vega Landing-Site Regions // Solar System Research. 2002. V. 36, No. 2. P. 136–159.
7 Ivanov M.A., Head J.W. Global geological map of Venus // Planetary and Space Science. 2011. V. 59. P. 1559–1600.
8 Ivanov M.A., Head J.W. The stratigraphic and geographic distribution of steep-sided domes on Venus: Preliminary results from regional geologic mapping and implications for their origin. // J. Geophys. Res. 1999. V. 104, № E8. P. 18907-18924.
9 Buchan K.L., Ernst R.E. Plumbing systems of large igneous provinces (LIPs) on Earth and Venus: Investigating the role of giant circumferential and radiating dyke swarms, coronae and novae, and mid-crustal intrusive complexes // Gondwana Research. 2021. P. 25–43.
10 Wilhelms D.E. Geologic Mapping in Planetary Mapping // Cambridge University Press (eds R. Greeley, R. M. Batson). 1990. P. 208–260.

## Maxe L.P. Shape and morphology of cosmic dust particles as manifestation of the adiabatic shift. UDC 524-1/-8

ALC «STRIM», Mogilev, Belarus, larissa_maxe@rambler.ru

**Abstract.** Among the cosmic dust particles (CD) accumulating on Earth in sedimentary deposits, in rocks, in addition to nano- and microspheres of various compositions, there are metal particles in the form of ribbons, chips, twists and even stacks of micro plates. Similarity was found in the shapes and morphology of these CD particles and particles of terrigenous and industrial origin, which is explained by a similar mechanism of their formation in fast flowing processes accompanied by a local adiabatic shift (AS). The paper considers the objects and conditions that can lead to the formation of CD in the form of shavings, twists and stacks of spall plates. Analyzing the manifestation of AS during the destruction of meteoroids, the author concludes that the shapes and morphology of the CD particles studied by him, studied and presented in scientific publications by various authors, are natural and are the result and manifestation of AS. Uncontrolled local AS leads to destruction, a controlled AS process can be used for synthesis an example is the use of vapor-bubble media.

***Keywords**: cosmic dust, local adiabatic shift, meteoroid.*

**Introduction**. Cosmic substance constantly enters the Earth's atmosphere and settles increasing planet's mass, the most significant part of it is cosmic dust (CD) – particles ranging in size from nano- to micrometers. CD particles differ in their sources of origin, geometric shape and morphology, chemical and elemental composition. In the composition of CD background, a part of the CD that is relatively uniformly and constantly present in sedimentary layers, excluding places of impact events, and except for nano- and microspheres of various compositions, are present many metallic particles in the forms of ribbons, shavings, twists, as well as scaly particles. It is not uncommon for deep magmatic rocks to contain inclusions of micro particles similar in shape and morphology to CD particles that accumulate in sedimentary rocks. Researchers recorded the presence of micro particles of native metals in them in the form of thin spirals, ribbons and shavings and it was difficult to prove their terrigenious origin without conducting special additional studies (Shnyukov, Lukin, 2011).

**Theory, practice, task.** High-resolution images of micro-objects are widely used for comparative analysis. Such research method as electron probe microscopy allows for both composition comparison and finding image similarity. For comparative analysis, in this work were used images of CD particles obtained earlier in the analysis of CD from various tablets-layers (Russia, Belarus) by scanning electron microscopy (SEM), as well as images of CD micro particles presented in published scientific papers by various authors and in open sources. Comparative analysis has shown the similarity of SEM images of certain shapes of CD particles with (obtained using SEM) images of particles of shavings from grinding and cutting (Zubarev, Priemyshev, 2021).

The discovered similarity of shapes and morphology of micro-particles from such different sources required explanation, analysis and search for the causes of similarity, respectively, was set in this work the task of analyzing the similarity of images, search for mechanisms of formation of CD micro-particles and their terrestrial prototypes.

Macro particles in the form of shavings are often found as waste from industrial processing of metals and other materials. Micro-sized shavings particles are formed in precision cutting, grinding and other processes. The theory of the process of mechanical processing of materials is in demand and by now its main provisions are well developed, adapted to specific types of processing and materials. Shavings formation occurs at a very high speed when materials are processed by cutting and grinding. At the point of application of the force causing the shear, as a result of the plastic deformation in a narrow zone, a significant amount of heat is released point-by-point, since the shear deformation is concentrated locally in this zone. This process in materials describes the mechanism of local adiabatic shear (AS), the condition of which is a rapid local cycle consisting of plastic deformation of the material, conversion of work into heat and thermal softening of the material. High-speed shavings formation proceeds cyclically. The cyclic nature of the process leads to the formation of adiabatic shear bands (Landau et al., 2016). Physically, they are realized directly in the material in the form of shavings: when cutting, an articular, cyclic, elemental one is formed, while grinding, a micro- shavings of similar types is formed (Zubarev, Priemyshev, 2021; Landau et al., 2016).

**Analysis of researches, similarity**. SEM images of CD particles similar in shape and morphology to industrial micro- shavings are given in many scientific papers, outside of the AS phenomenon. The ablation of a cosmic body (meteoroid) in the Earth's atmosphere proceeds at a very high speed, the duration is measured in seconds, the outer layers are subjected to high–temperature ablation, the inner ones do not immediately have time to heat up the body is exposed to the shock wave front. During the atmosphere stage of evolution of a heterogeneous cosmic body by deceleration and destruction internal friction between dissimilar parts and particles is possible. Solid minerals, during shifts and shocks, as abrasives, remove shavings from metal inclusions, in this case, the AS phenomenon is reflected on the CD particles – they take the form of corrugated, elongated or folded ribbons, spirals. An increase in the cutting speed during material processing reduces the size of the shavings of grinding metal, longitudinal grooves from plastic deformation, scaly delaminations, ruptures, voids become noticeable on the particles. Similar phenomena are observed on CD metal particles (Tselmovich, Maxe, 2020; Tselmovich, Maxe, 2023). Using USB-microscopy (with registration of color images), the author conducted studies of CD particles extracted from native dry trepel (Stalnoye deposit, Khotimsk, Belarus). On USB-images of CD particles similar to micro-shavings, the presence of run colors (analogue to colors of the run on the metal), from yellow to blue, was recorded on their side surfaces, therefore, the shavings formation temperature could vary but without reaching the Curie point.

Penetrating into the upper atmosphere, space bodies undergo ablation, leaving ionized meteor trails at an altitude of 70 to 140 km these tracks are capable of reflecting and scattering radio waves of high frequency and ultrahigh frequency range. Massive cosmic bodies, before an explosion, fall or successful crossing of the atmosphere, leave long-lived meteor trails in it. Scientists and specialists from many countries monitor various layers of the atmosphere, including the observation of "metallic" layers, the ionic composition of which correlates qualitatively and quantitatively with the metals that make up falling meteorites (Plane et al., 2015). Intensive targeted studies have led scientists to the conclusion that relatively large meteoroids are the main source of micrometer-sized meteorite dust settling on Earth, which accumulates and can persist for a long time in sedimentary deposits, becoming as background CD (Klekociuk et al., 2005).

CD particles observed in the form of shavings, ribbons, patterned leaves with traces of viscous flow and metal destruction could be formed as a result of internal processes (deformations, friction) in an inhomogeneous meteoroid body during and even before it enters the Earth's atmosphere. Similar particles could have been formed during the cosmic evolution of the object, as evidenced by the result of a high-altitude explosion in the atmosphere recorded in 2004 and the analysis of its trace (Klekociuk et al., 2005).

During the ablation of the meteoroid, the melt can carried away by a plasma stream and evapourate, but also in area its back side vacuum, the metal melt under pressure can be displaced through cracks in refractory phases, forming flow-scaly forms of CD particles resistant to corrosion like amorphous metal glasses (Tselmovich, Maxe, 2023).

The formation of assembly of particles in the form of a regular "stack of plates" (more similar to stacked micro-saucers) obviously require quite other but also extreme conditions. The appearance of localized deformation shifts and the formation of periodic structures in metals under shock and pulsed action have been mathematically and experimentally proved (Buravova, Petrov, 2020).

For space objects entering the Earth's atmosphere, explosion and impact are a factor of destruction with extreme conditions of fragmentation and formation of both macro debris and micro-particles of CD. Impact during the fall and explosion of meteorites create conditions form deformation shifts, local bands of AS (as zones of interference of unloading waves). CD micro-particles in the form a stack of spall micro-plates (an assembling of micro saucers) are found on Earth (and found on the Moon) in places of explosion and fall of meteoroids. Based on the conditions, it is most likely that CD particles in the form of spall micro-plates are formed when a shock pulse is applied to thin metal veins in the structure of meteoroids, since their terrestrial prototypes – spall plates in experiments are formed under the action of a shock wave in metal foils, in thin rods and wires (Buravova, Petrov, 2020). The presence of particles in the form of spall micro-plates in the research material, including CD, can be considered a diagnostic sign of a catastrophic type of event, since they are the result of the impact of shock waves on metal inclusions, reflection and interference of waves in a finite closed object – a manifestation of local AS.

**Analysis and discussion. The phenomenon of ejection.** In addition to the explosive scattering of fragments and micro particles contained in the body of the meteoroid, there is a "legitimate" possibility of carrying its particles into the external environment. Due to the ejection created by an annular jet of an external plasma stream at supersonic speeds, a part of the substance can be carried away from its rear region into the atmospheric trace of a meteoroid. The presence of low-frequency oscillations of the bottom jet was shown, since its oscillations are slower than high-speed turbulence in the mixing plasma (external), that is, they are slow and periodic (Bulat, Prodan, 2013). In the absence of air inside the meteoroid, its own "vacuum pump" – an ejector – can operate in its back rear area. The position of the back vacuum end of the meteoroid by rapid motion in atmosphere is not stable, but under certain conditions it can function as an ejector of small fragments and particles. From inside the meteoroid, the "tail ejector" can periodically "spits out" shaken and cracked substance. Regmaglypts are observed on some meteorites, indicating uneven pressure and flow. The presence of a bottom vacuum and the loss of matter in the bottom region affect the shape of iron and iron-stone meteorites that have reached the Earth: there is a rear section and a pointed nose, behind which are side tightness (the so-called "ears") protrude.

**Analysis and discussion. The crust of melting. Diamonds in the local AS.** Scientists have identified the study of the composition and structure of the crust of melting of meteorites as a special, information-oriented direction (Scott et. al., 2023). In connection with the task of searching for internal friction particles, it is convenient to consider the fixation of expected particles, if any, in the crust of melting. The opportunity to study the thick crust of melting was provided by the Chelyabinsk meteorite. A small fragment of it was transferred to the Geophysical Observatory Borok (RAS) for microprobe analysis using Tescan Vega II. The crust of melting, which passes into the inner part untouched by thermal heating, makes it possible to analyze and compare, given that there was melting, but the melting crust was still absent during the movement of the meteoroid. Cooling down, the fragment of the meteoroid recorded the current state and results of physical and physico-chemical processes in the structure, shape and morphology of particles, and the composition of compounds. Assuming that particles whose origin is due to internal processes involving friction can be fixed in the crust of melting of meteorite, the study was carried out using a gentle method.

For petrography analysis, polished slips are usually used, which allow to get an image of some part of the object. In a result are observed and fix an image of polished surfaces that include objects in one plane. For volumetric SEM "visualization" a powder by soft separation of the small part of the crust fragment was used. Particles in the form of twists and cylinders were found in the powder representing the central part of the crust of melting. Such particles from inside of crust can be considered the result of fixation of physical and physico-chemical processes that were occur in the crust of melting before the explosion of the meteoroid. Their formation was took place under conditions of high dynamic loads, high-speed ablation of the outer part of the meteoroid, the highest temperature gradient in a narrow layer between the outer and inner non-heating part, the crust was subsequently formed during very rapid cooling (Tselmovich, Maxe, 2023*).

Destruction of cosmic bodies is a short–term, high-speed process with various manifestations of AS: accompanying nano- and micro carbon particles of various allotropic forms are often found in CD particles as inclusions and near the particles of CD. Until recently, the explanation was only the shock or explosive mechanism of the formation of micro crystals of Moissanite, diamonds, since the explosion method can produce particles of different sizes – mixes of micro diamond or films. Currently, a technology has been developed for the synthesis of diamond nuclei using bubbles of a vapor–bubble medium (Fomin, 2021). Judging by the description in the Patent, the bubble method for producing nano- and micro-diamonds makes it possible to explain the presence of inclusions of nano- and micro-diamonds in and on the surface of particles of CD even they were not subjected to shock loads. According to invention the cavitation conditions are created in the flow of carbon-containing liquid and steam, the process proceeds when the bubble space collapses: nano- and micro-diamonds are formed under conditions of local AS, but already as a synthesis product (Voropaev, Dushenko, 2021).

**Conclusions.** A comparative analysis of SEM images, practice and theory of AS allowed us to establish the similarity and manifestation of local AS in CD particles, to explain the mechanism of their formation. The shapes and morphology of CD particles found in sediments and rocks presented in many scientific papers are natural, and are due to the manifestation of AS in the process of destruction of cosmic bodies in the atmosphere and on Earth. The analysis of the processes of formation of micro-particles for compliance with the conditions of local AS allows us to assume possible variants of particle shapes, since the operation of many industrial devices is accompanied by the formation of micro particles. Their sources can be both arc devices and plasma torches, as well as particle accelerators and plasma engines, the smallest dust particles are formed during the movement of elements, joints, parts of vehicles, including space ones. An uncontrolled local AS leads to destruction, a controlled or controlled AS can be used for synthesis. Vapor-bubble environments, phenomena, and end products observed in natural processes on Earth are also likely in cosmic bodies, for example, comets. In CD samples isolated from various samples, particles specific shapes (mesh and "bubble") are found, they are observed both in ablation products and in the melting crust of meteorites. Micro particles of destruction and synthesis formed under conditions of local AS require further study and practical applications.

*The author expresses his deep gratitude to the lead scientific employee of Geophysical Observatory Borok Inst. Physics of Earth RAS Ph.D. Tselmovich V.A. for help to my efforts and my involvement to the investigations into CD area, cooperation and big scientific and practical assistance in the analysis of CD.*

**References**

Bulat P.V. On the low-frequency oscillations of expenditure base pressure / P.V. Bulat, N.V. Prodan // Fundamental research. – 2013. – № 14 (part 3) – pp. 545-549.

Buravova S.N., Petrov E.V. Microstructure of metal in spall plates. Chemical Physics, 2020, volume 39, № 9, pp. 63-70.

Fomin P.A. Explosive and detonation processes in chemically active bubble media: Monograph. / P.A. Fomin, I.B. Palymsky, S. Gareidash, V.S. Hayrapetyan. – Novosibirsk, SSUGiT, 2021, P -160.

Klekociuk A.R., Brown P.G., Pack D.W., ReVelle D.O., Edwards W. N., Spalding R.E., Tagliaferri E., Yoo B.B. & Zagari J. Meteoritic dust from the atmospheric disintegration of a large meteoroid. NATURE. Vol 436|25 August 2005. Letters. P. 1132 – 1135. doi:10.1038/nature03881.

Landau, P., Osovski, S., Venkert, A. et al. The genesis of adiabatic shear bands. Sci Rep 6, 37226 (2016). https://doi.org/10.1038/srep37226

Plane John M. C., Feng Wuhu, Dawkins Erin C. M. The Mesosphere and Metals: Chemistry and Changes. (2015). Chemical Reviews, 115(10), 4497 – 4541. doi:10.1021/cr500501m.

Scott J.M., Negrini M., K. Faure K., Palmer M. C., Knaack D. R., Leybourne M. I. Multi-zone fusion crust formation and classification of the 2004 Auckland meteorite (L6, S5, and W0) / Meteoritics & Planetary Science 58, Nr 3, 328 – 340 (2023).

Shnyukov E.F., Lukin A.E. On native elements in various geo-formations of the Crimea and adjacent regions.

Geology and Minerals of the World Ocean, 2011, No. 2, pp. 5-30.
Tselmovich V.A., Maxe L.P. Microstructure and composition of particles of native iron of cosmic origin. Proceedings of the All-Russian Annual Seminar on Experimental Mineralogy, Petrology and Geochemistry (RASEMPG–2020). M. 2020. pp. 278-281.
Tselmovich V.A., Maxe L.P. Recognition of cosmic and atmospheric dust particles. Proceedings of the All-Russian Annual Seminar on Experimental Mineralogy, Petrology and Geochemistry (RASEMPG-2023). Moscow. 2023. / Editor–in-chief O.A. Lukanin, Moscow: GEOCHE RAS, 2023. pp. 347-351.
Tselmovich V.A., Maxe L.P. Spherical and cylindrical forms of minerals in the thick melting crust of a fragment of the Chelyabinsk meteorite. Materials of the XIII All-Russian Youth Scientific Conference "Minerals: structure, properties, methods of researches". Yekaterinburg, 2023*, pp. 291-293.
Voropaev S. A., Dushenko N. V. A method for producing ultrafine diamonds and an installation for its implementation. RU (11) 2784236(13) C1. 2021.
Zubarev Yu.M., Priemyshev A.V. Theory and practice of improving the efficiency of grinding materials. Publishing house "Lan", 2021, p – 304.

## Mukhamedzhanova A.E. Valley topography of northeastern Terra Cimmeria on Mars. *UDC 523.4*

Vernadsky Institute of Geochemistry and Analytical Chemistry, RAS, Moscow, alinam2001@gmail.com

**Abstract**: On Mars, there are landforms that visually resemble river valleys and watercourse beds. One of the possible explanations for this fact is the fluvial character of these formations, suggesting the presence of liquid water as an agent of formation of this kind of relief. The purpose of this work is to identify the most probable variant of the origin of the valleys of the northeastern Terra Cimmeria. The main characteristics of the network were obtained: valley lengths, widths, and gradients, as well as morphological characteristics of the valleys: longitudinal profile, depths and widths along the banks and bottoms, and the shape of the transverse profile. Changes in the shape and parameters of the cross-sectional profile down the valleys were also analyzed to elucidate the patterns of valley development. The study revealed that both valley systems are characterized by branching (presence of watercourses of several orders) together with weak development of upper links of the erosion network. Both main valleys tend to develop a U-shaped profile and to widen their bottoms as they approach the mouth. Correlative landforms (outcrop cones, terraces) in the Ma'adim valley may indicate flowing water activity. Most likely, the considered valleys were formed by relatively fast deep erosion by geologic standards.

***Keywords:*** *Mars; Terra Cimmeria; river valleys; valley forms; fast deep erosion.*

**Data and methods** The purpose of this paper is to identify the most likely variant of the origin of the valleys of the north-east of the Terra Cimmeria. The main methods used in the work are geomorphological interpretation of Mars remote sensing data and morphometric measurements using GIS technologies. The methodology for studying valley forms included: deciphering valley thalwegs, studying the structure of the valley system, studying the morphology of individual valleys, studying the relationship of valleys with landforms of a different genesis. Based on the global geological map of Mars (Tanaka et al., 2014), the geological map of the Aeolis quadrant (Scott et al., 1978), as well as visual interpretation of CTX space images with a spatial resolution of 6 m, it was revealed that the northeast of the Terra Cimmerian is a combination of plains of various morphologies significantly reprocessed in Hesperian and Amazonian Epochs by complex denudation and impact-explosive processes, formed on ancient (presumably Early and Middle Noahic age) rock complexes. These plains are cut through by two submeridionally oriented valley systems – Ma'adim and Durius.

**Results:** During decoding, the structure of the valley system was encoded. In this case, the Strahler system of determining the order of valleys was used, where each tributary of the river is classified in accordance with its position in the overall system. (Fig. 1).

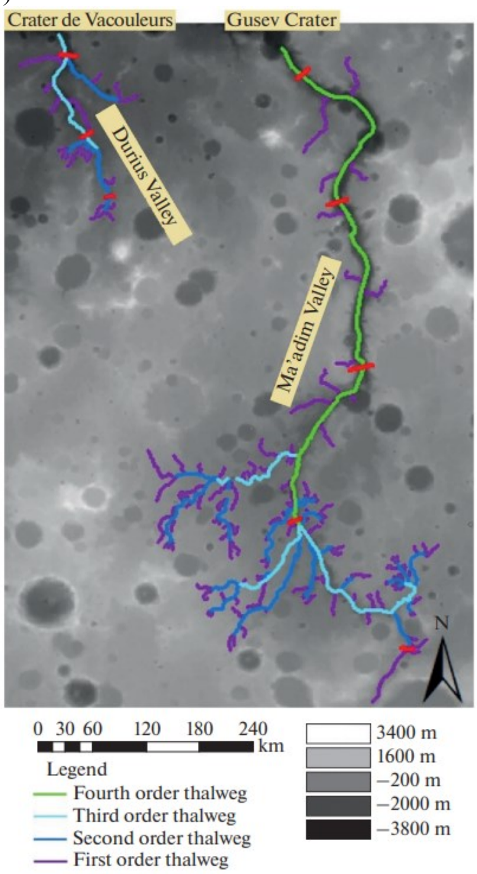


**Fig. 1.** Ma'adim and Durius valley systems in the MOLA DEM image (spatial resolution 463 m/px).

A set of characteristics that helped identify and describe this type of relief was used as deciphering features of valley forms. For example, narrow and deep valleys indicate that the conditions for the formation of such forms existed for a short time, but with active processes of incision. Wide valleys indicate a long time of their formation. In some cases, valleys have a fairly clear appearance, from which their structure, pattern and morphology can be determined. Thus, both in the Ma'adim Valley system and in the Durius Valley system, the main valleys and their tributaries are clearly distinguished by shape, size, and albedo.

The main characteristics of the system were obtained: the lengths of the valleys, their width, slope, as well as the morphological characteristics of the valleys: longitudinal profile, depth and width along the edges and bottom, shape of the transverse profile. The change in the shape and parameters of the transverse profile down the valleys was also analyzed to clarify the patterns of valley development.

The morphological characteristics of the valley can be characterized by studying its longitudinal and transverse profiles (Fig. 2, Fig.3).

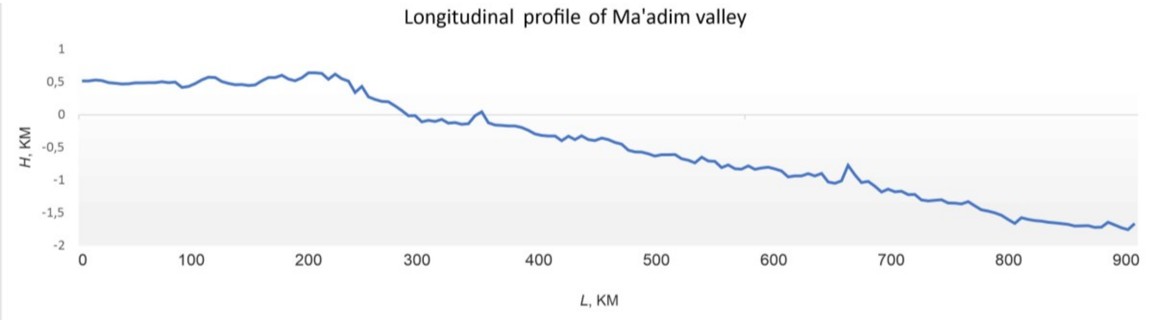


**Fig. 2.** Longitudinal profile of the main valley of the Ma'adim valley system based on MOLA DEM data (spatial resolution 463 m/px), where L is the distance along the profile and H is the height;

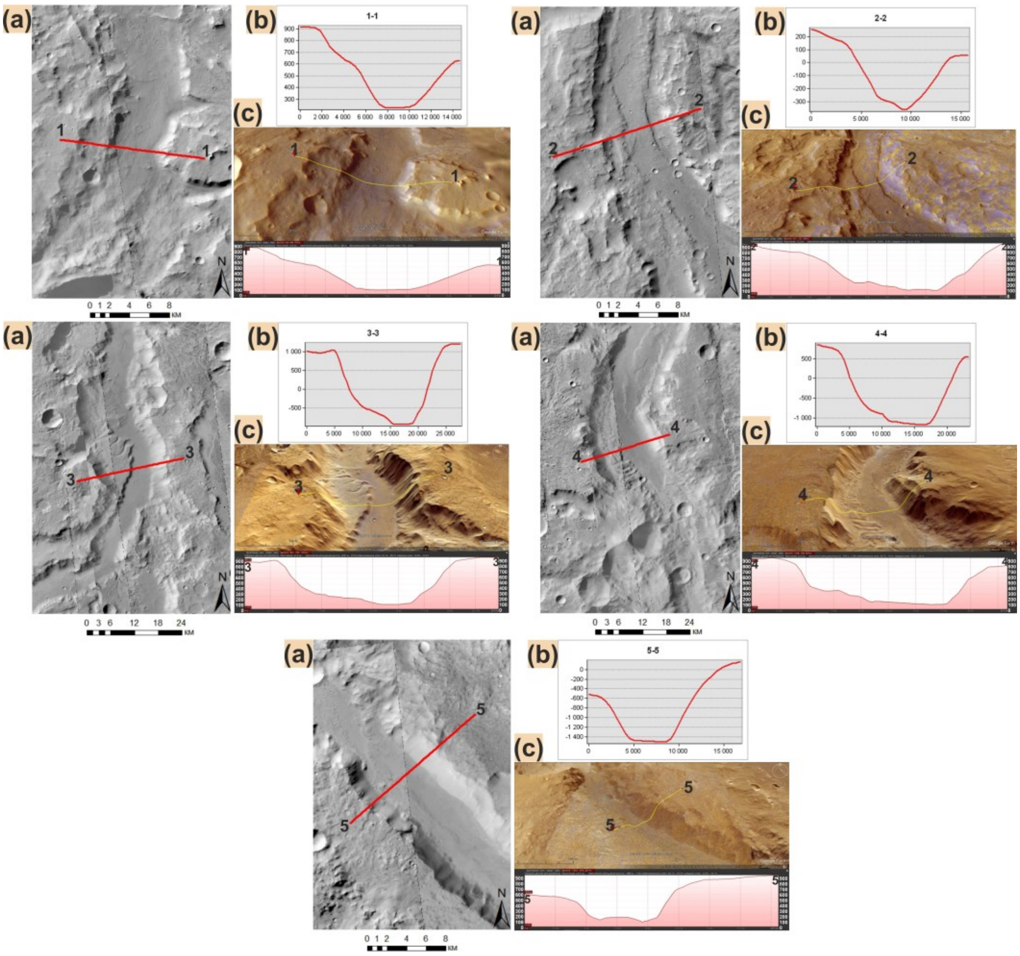


**Fig. 3.** Transverse profiles 1-1–5-5 of the main valley of the Ma'adim Valley system: based on CTX images (a); MOLA DEM (b); and based on HRSC DEM obtained on the Mars Express spacecraft (c).

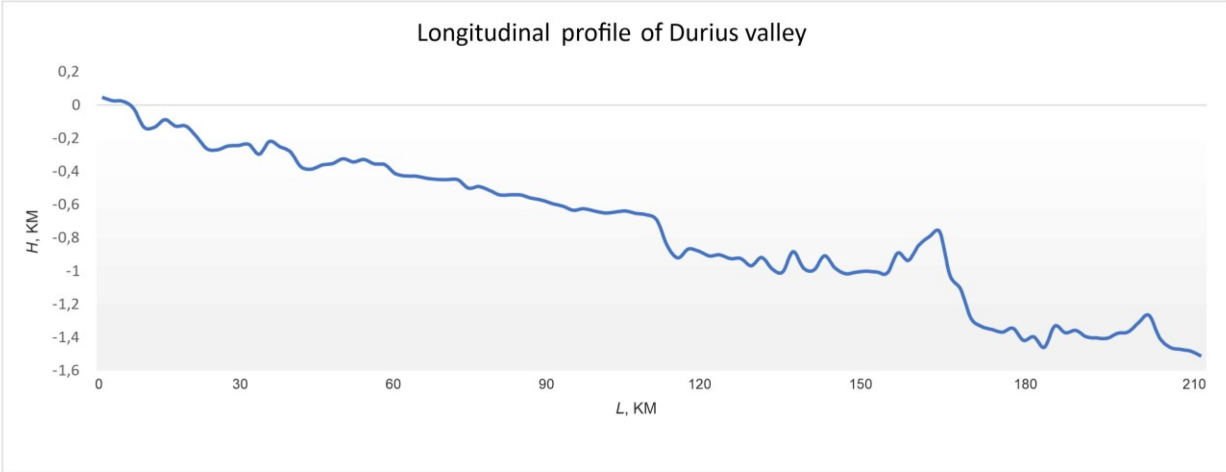


**Fig. 4.** Longitudinal profile of the main valley of the Durius Valley system based on MOLA DEM data (spatial resolution 463 m/px), where L is the distance along the profile and H is the height;

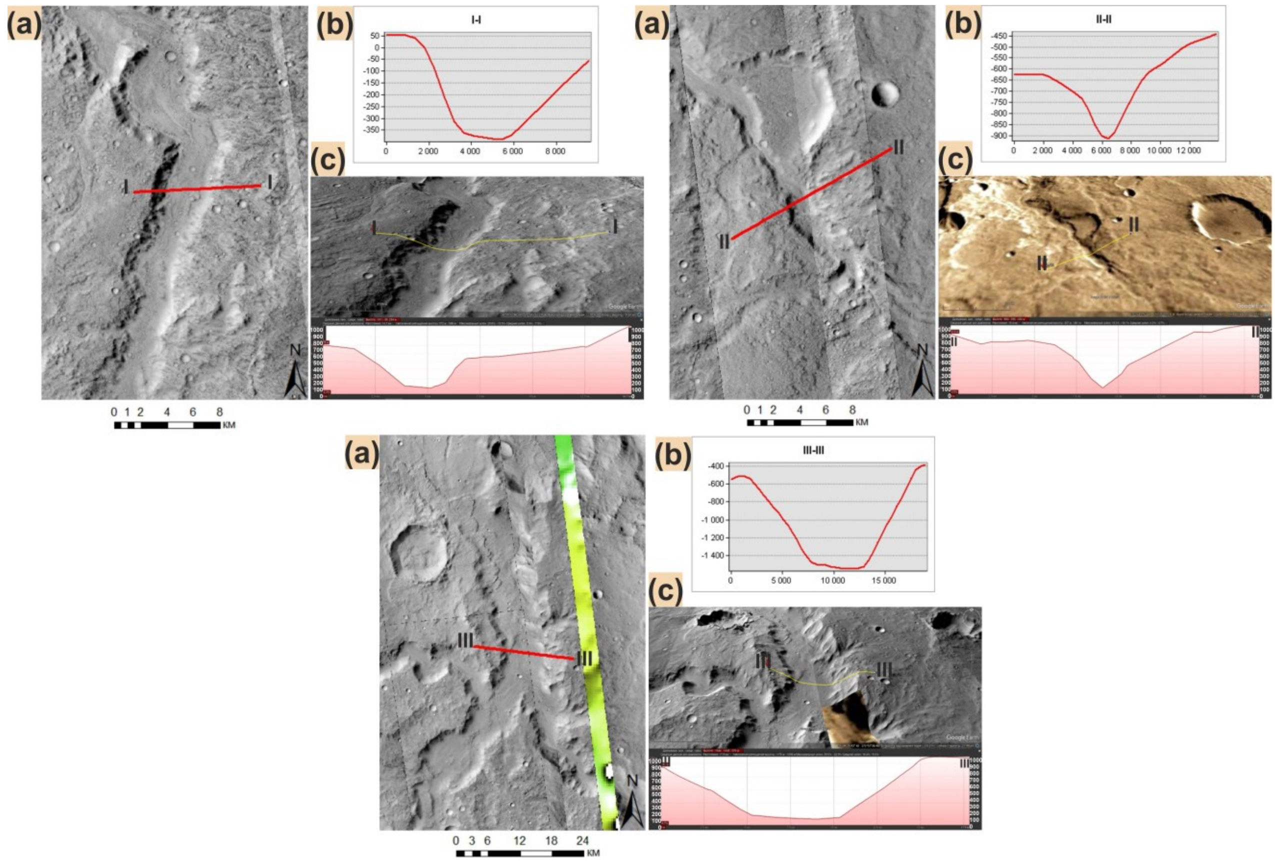


**Fig. 5.** Transverse profiles I-I–III-III of the main valley of the Durius Valley system: based on CTX images (a); MOLA DEM (b); and based on HRSC DEM obtained on the Mars Express spacecraft (c).

The morphological characteristics of the Durius valley can be also characterized by studying its longitudinal and transverse profiles (Fig. 4, Fig.5).

**Discussion and conclusions:** During the study, it was found that both valley systems are characterized by branching (the presence of watercourses of several orders) in conjunction with the weak development of the upper links of the erosion system: tributaries of low orders have a short length and insufficient morphological expression compared to the main valley. A general trend of incision from south to north was revealed. Both main valleys tend to develop a U-shaped profile and widen the bottom as they approach the mouth. Correlated landforms (fans, terraces) in the Ma’adim Valley may indicate flowing water activity.

The valleys cut through the surrounding plains, composed of rocks of early and middle Aachian age, which indicates a younger age of the valleys. There are areas where valley systems were partially destroyed as a result of impact events, and a rather low morphological preservation of the Ma'adim Valley paleodeltae is observed. These facts allow us to assume a fairly ancient origin of the valley and the cessation of its active functioning even in pre-Amazonian Epochs.

Thus, the most likely time period for the formation of these valley systems seems to be Late Aachian– Early Hesperian Epoch, which does not contradict existing estimates for some other valleys. Most likely, the valleys considered were formed due to relatively rapid (by geological standards) erosional incision.

*This work was supported by the Vernadsky Institute of Geochemistry and Analytical Chemistry of the Russian Academy of Sciences.*

### References

1 Scott D. H., Morris E. C., West M.N. Geologic map of the Aeolis Quadrangle of Mars // U.S.G.S. Misc. Inv. Map 1-1111, 1978.

2 Tanaka K.L. et al. Geologic map of Mars: U.S. Geological Survey Scientific Investigations Map 3292, scale 1:20,000,000 // U.S.G.S., 2014, p. 43.

## Portnov A.M. Fracture-shock morphology of the Mars surface and interpretation of its magnetic and gravitational fields

MGRI , Moscow, portnov@mail.ru

**Abstract**. Stable maghemite is an indicator of shock events on the Earth and on Mars. After the publication in the last century of magnificent images of Mars taken by NASA's Viking-2 probe, we came to the conclusion that the Red Planet's ecosystem was destroyed by an asteroid impact when the huge astroblem "Plain Hellas" was formed. An indicator of the presence of the former ecosystem remained "red-colored weathering crust", consisting of iron oxides, the thickness of which is estimated at 100 m and which took, according to our calculations, 500 trillion tons of free oxygen of the atmosphere of Mars (1). "Red-flowers" occur in warm, humid climates. For comparison, we note that there are 1200 trillion tons of O2 in the Earth's atmosphere.

***Keywords**: gravitational and magnetic fields of Mars, astroblems Hellas, Argyre, Popigai, maghemite, thorium-magnetic aeroanomalies, gold, platinoids, REE.*

The surface morphology of Mars is defined against the background of numerous craters by the impact of the huge astroblems Hellas and Argyre. They created a cross-shaped direction of planetary faults. These include shock-tectonic faults of NW direction (Mariner fracture - "volcano" Olympus) and NW direction, expressed in the linear structure of the other "volcanoes" (Fig. 1 - "Volcano" Olympus), with a volume of about 4 million km³ (Fig. 2) and other "volcanoes" are not reflected, as is typical for such objects, in the maximums of magnetic and gravitational fields (Figs. 3, 4).

Color-coded Elevations on Mars, MOLA Altimeter, MGS Mission

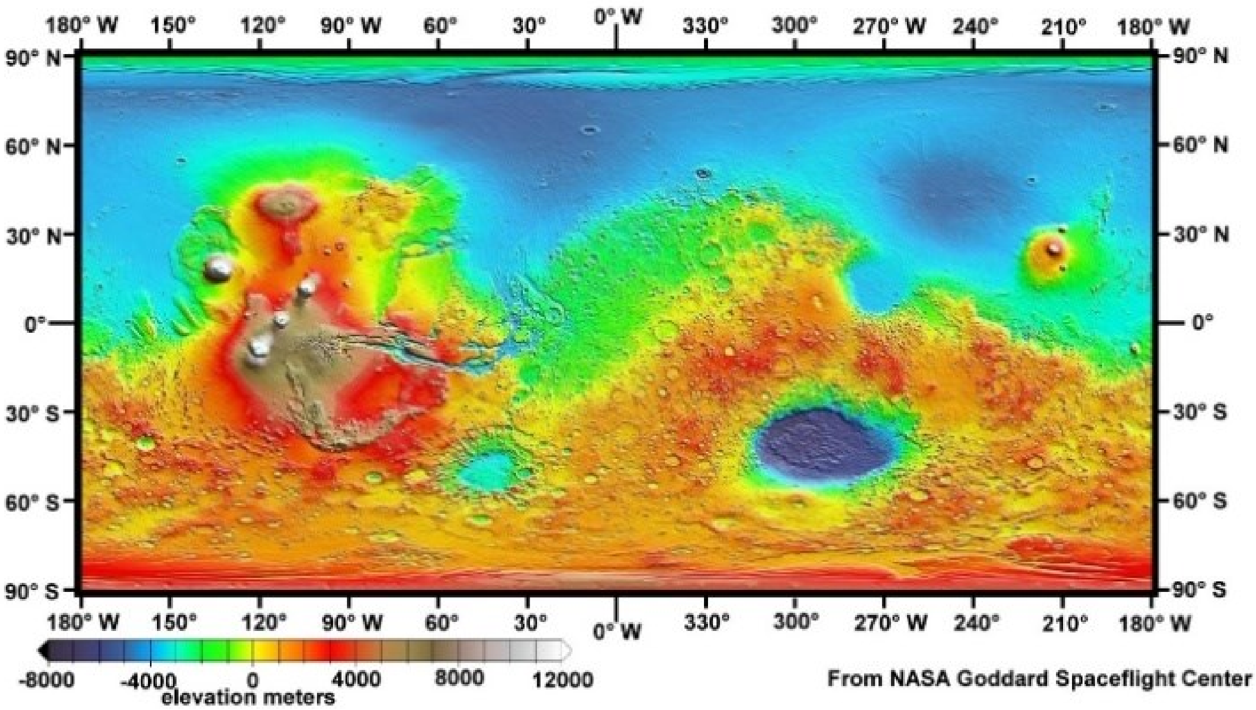


**Figure 1.** The surface of Mars is defined by the Hellas and Argyre astroblems. Magnetic (with maghemite) emissions of astroblems are reflected by the maximum of the magnetic field of Mars.

**Figure 2.** Geyser Olympus, the highest ice mountain (26 km) on the planets of the Solar System. It is not reflected in the magnetic field of Mars (Fig. 3) and has a low gravitational field (Fig. 4), indicating an ice composition. The character of the lower part of the solar (southern) slope demonstrates its melting and collapse.

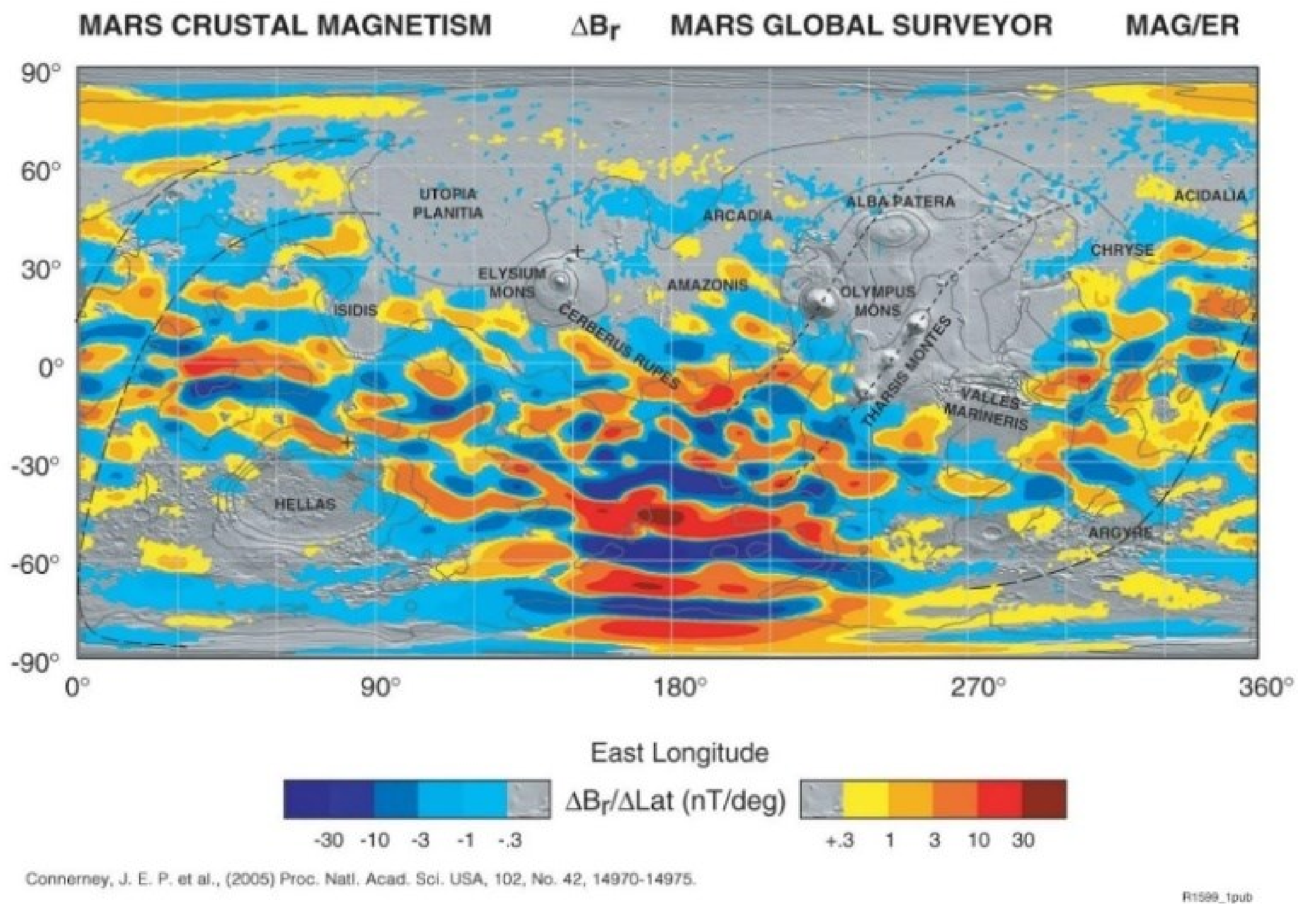


**Figure 3**. Map of the magnetic field of Mars. NASA, Mars Orbiter Surveyor probe. 2005 г. The altitude of the orbit during imaging is 400 km. We attribute the high level of the magnetic field near the South Pole to ejections from the giant astroblems Hellas and Argyre (Fig. 1). The spotted field is water-aeolian variations of the dusty material of emissions. The low magnetic and gravitational fields of the so-called "volcanoes" (Olympus et al., Figs. 3, 4) are characteristic, which allows us to attribute the mountains to ice structures of superpowered geysers.

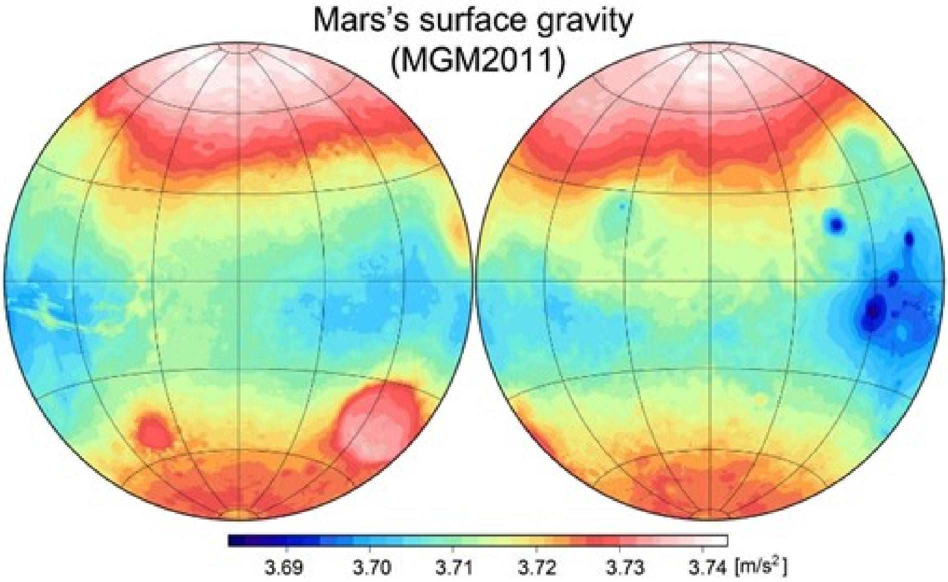


**Figure 4.** On the background of the abundance of impact craters on the small-scale gravimetric map of Mars, only two "plains" stand out - Hellas (probably a fallen satellite, named by us, "Thanatos" ("Death"), like Phobos, which destroyed the ecosystem of Mars) and Argyre (dimensions see in the text). NASA data. In our opinion, the two giant astroblems created the catastrophe that defined Mars landforms such as the giant Mariner fissure and the ice geysers Olympus et al.Magnetic field compiled by NASA's Mars Orbiter Surveyor probe in 2005. The orbital altitude at the time of imaging was 400 km. The low spotty magnetic field is formed by water-aeol varieties of dusty emission material, their intensity is 800 times weaker than the Earth's magnetic field. In our opinion, the "volcanoes" are ice geysers, since they are located only in low magnetic and gravitational fields.

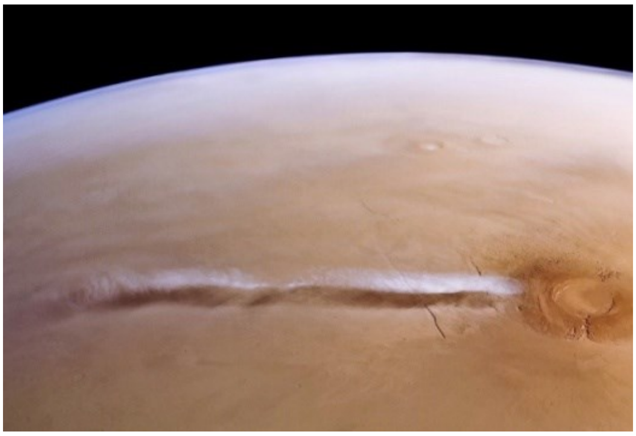

**Figure 5. A** grandiose release of water vapor over 2000 km long by one of the "volcanoes" in 2020 confirms their geyser (water) type of volcanism**.**

The emissions of the Hellas and Argyre astroblems are reflected by the maximum of the magnetic field of Mars (see Fig. 2). The Hellas plain has a diameter of 2300 km (!), a depth of 9 km, and emissions of > 35 million km³. The Argyre Plain has a diameter of 900 km, a depth of 7 km, and emissions > 4 million km³. Massifs composed of calcined emissions contain up to 5-15% maghemite, according to NASA Mars rover data. Maghemite mineral is magnetic, gamma-$Fe_2O_3$, and has a spinel structure (Fig. 6). The magnetic region near the South Pole of Mars is associated with an abundance of calcined emissions in a total huge volume (.> 40 million km³ of soil !).

**Figure 6.** Stable maghemite, gamma-Fe2O3, magnetic, spinel structure, ao=0.832 nm. Schlich with grain size 0.5-2.0 cm from the Vilyui River, with Ir, Pt, Pd Au, TR,Stable maghemite, gamma-Fe2O3, magnetic, spinel structure, ao=0.832 nm. Schlich with grain size 0.5-2.0 cm from the Vilyui River, with Ir, Pt, Pd, Au, TR.

Similar in intensity magnetic anomalies with maghemite were also established by us in the process of aerogeophysical survey in the Vilyui River basin, on the southwestern margin of the Popigai astroblem periphery (2,3). Maghemite from Vilyuy is cubic, a0 =0.832 nm, it is unusual in the composition of impurities and contains Th 80 g/t, the sum of REE 0.3%, impurities Au, Ir, Pt, Pd. The refractory composition of impurities indicates, in our opinion, the formation of maghemite from high-temperature plasma (see Fig. 6). Maghemite on Mars probably has a similar genesis.

The Mariner fissure is 4000 km long, up to 200 km wide, and up to 12 km deep and is characterized by solifluction, i.e., the presence of a grandiose mud flow with the dissolution of collapses of thawing frozen ground in salty liquid mud (Fig. 7). The depth of the mud flow reaches 1 km. Mariner Crack is the warmest place on Mars. Collapses of soil from the slopes indicate that warming is going on not only on Earth, but also on Mars. In my opinion, warming is evident on all planets of the solar system, but on Mars it looks most clearly.

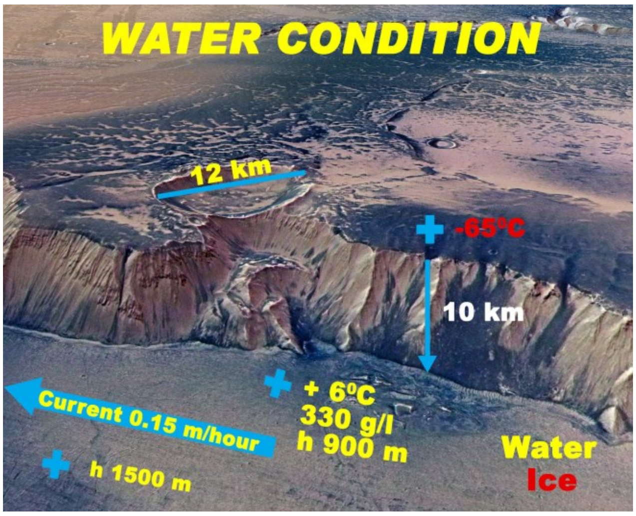


**Figure 7.** Grandiose solifluction saline flow in the "warming zone" -- Mariner fracture. The state of water and solution was evaluated by Associate Professor A.Naravas (MGRI - RGGRU) (4).

**References**

1. Portnov A. M. How life on Mars perished. Science and Life, 1999. №4. C.92-96.
2. Portnov A. M. Golden rain of astroblems. Priroda, 2021, No.2. C. 31-40
3. Portnov A. M. Apocalypse on Mars. Ridero. 2016. C.116.
4. Naravas A.K. Praktika biolocatsiya v geologii [The practice of biolocation in geology]. M., ed. "Print PRO". 2016 . C.108

## Tselmovich V.A.[1], Shelmin V.G.[2], Maxe L.P.[3], Kurazhkovskii A.Yu.[1] Microscopic traces of the Chulymskiy bolide (falling of 1984, point 1, Minaevka). *UDC523.64*

[1] GO "Borok" IPE RAS" tselm@mail.ru, [2] Ecomonitor LLC, Tomsk, chulymmb@mail.ru, [3] ALC "STRIM", Mogilev, Belarus, larissa_maxe@rambler.ru

**Abstract.** On February 26, 1984, an explosion of a space object, the Chulymsky bolide, occurred in the Chulym River area on the border of the Krasnoyarsk Territory and the Tomsk Region. The study of the first fragments found in the explosion area did not give encouraging results regarding belonging to meteorites. A cometary version of the nature of the Chulymsky cosmic body (CCB) has been adopted with the intention of finding "traces" of the bolide comet - microscopic cosmic particles that are well preserved in swamps. An initiative expedition was undertaken to collect samples with suspected "traces" of cometary matter. Particles extracted from samples taken at point 1 of the CCB track near Minaevka were studied. The authors attributed some of the detected particles to the substance of the bolide destroyed by the explosion and believe that the Chulymsky bolide is a fragment of a comet–like space object. Among the mass of particles isolated from the "trace" of the CCB, aluminosilicate microspheres with a unique microstructure were found, turning into nanostructural features that do not occur in particles of volcanic emissions and are not formed in man-made processes.

***Keywords***: *Chulym space body, traces, bolide, comet, microspheres.*

**Introduction.** Meteorites have been of interest to mankind for a long time; they were used practically, but science is interested in them as objects in which information about the history of our Solar System is encrypted. Fragments of meteoric bodies and their study are the most important source of knowledge about the evolution of the Universe, Galaxy, Solar System and planets. The substance of meteorites and comets is especially valuable for science, since it contains particles that were formed in dust accumulations even before the formation of the Solar System; studying the composition of such pre-solar particles allows us to clarify the theory of the processes of formation and evolution of stars. “Primitive” meteorites, remnants of planetesimals, comets and their fragments contain primary chemical compounds, nano- and microparticles from which the Solar System was formed.

The Chulym cosmic body entered the earth's atmosphere on the evening of February 26, 1984. It flared up in the atmosphere on the border of the Krasnoyarsk Territory and the Tomsk Region and exploded at an altitude of about 10 km in the area of the Chulym River (a tributary of the Ob River). The passage of the fireball as an extremely bright object was observed for about 10 seconds and was accompanied by a shock sound wave and a micro-earthquake that was recorded by regional stations of the Unified Seismic Observation Network. In the summer of 1984, an expedition from the Institute of Geology and Geophysics of the Siberian Branch of the Russian Academy of Sciences was sent to the site of the CCB fall. The search for fragments of the cosmic body took place in the valleys of the Chulym, Bolshaya and Malaya Yuksa, Tunguska, Lai rivers, and also searched in the “Tunguska Triangle”: the village of Tungussky Bor, the village of Baturino and the village of Kayluska (Pervopashinsk). Then the expedition did not find any traces of a cosmic body in the indicated territory, and no broken fall of the forest were found either. At the same time, an analysis of eyewitness accounts was carried out, based on interviews with several hundred people. Scientists' conclusions about CCB, made in 1984, are based on these eyewitness accounts and are purely hypothetical. Initiative expeditions continued.

The version closest to the authors is based on the assumption that both the Chulym and Tunguska cosmic bodies were part of the group of bodies accompanying Halley's comet and could be its fragments (Voitsekhovsky, 1990). In this case, they could consist of low-density matter (for comets - less than 1 g/cm3), it included ice, gas condensates, solid particles - cosmic dust (CD). The power of the explosion of the Chulym bolide turned out to be much less than the Tunguska object (about 11 kilotons). The flight of the CCB was observed from east to west. The car "sparked" at a high altitude and fragments were separated from it until the final stage of the flight. Along the flight path during V. Shelmin's expedition in 2022, a scattering of debris of unknown origin was discovered, but there was no reason to attribute the found samples to fragments of the fireball.

The expedition of the Institute of Geology and Geography of the Siberian Branch of the USSR Academy of Sciences in the summer of 1984 and other amateur expeditions searching for fragments of an exploded cosmic body did not find fragments or evidence that could be unambiguously associated with the hypothetical composition of the fireball substance, so it was proposed to continue the research with a new goal. V. Shelmin organized an initiative expedition to search for microscopic traces of the Chulym explosion in the territory along the route of the object's flight.

Studies of dust particles ejected during flybys of a comet with a highly non-spherical nucleus, Comet 1P/Halley, have suggested that the dust has a varied composition. Observations of Comet Hale-Bopp (Levasseur-Regourd et al., 2018) showed that particles emitted from the nucleus contain silicates (forsterite), crystalline magnesium-rich pyroxenes, and amorphous silicates. The discovery of crystalline forms in the spectra of comets indicates that cometary dust minerals have been exposed to high temperatures in their history. The most important information was provided by samples with 81P/Wild 2. About 1% of the recovered particles turned out to be complexes of refractory minerals rich in Ca and Al, similar to inclusions in chondritic meteorites, possibly high-temperature condensates. In the 81P/Wild 2 samples, small amounts of minerals that formed as a result of exposure to water - magnetite (Mt) grains - were identified; no hydrated silicates were isolated, but "igneous rock" minerals cooling from melts were detected (Levasseur-Regourd et al., 2018).

Taking into account these studies of cometary material, we set the task of searching, along the flight path of the Chulym bolide, for microparticles distinguished by unusual morphology and composition, such that could be attributed to direct or transformed cometary matter. Considering that the matter of comets is extremely diverse both in the initial composition and in the composition of fallen and newly formed particles, earlier, when studying peat from swamps along the flight path of the Uchur bolide, particles with thin Ni-films were proposed as a diagnostic sign of cometary material (Tselmovich et al., 2023).

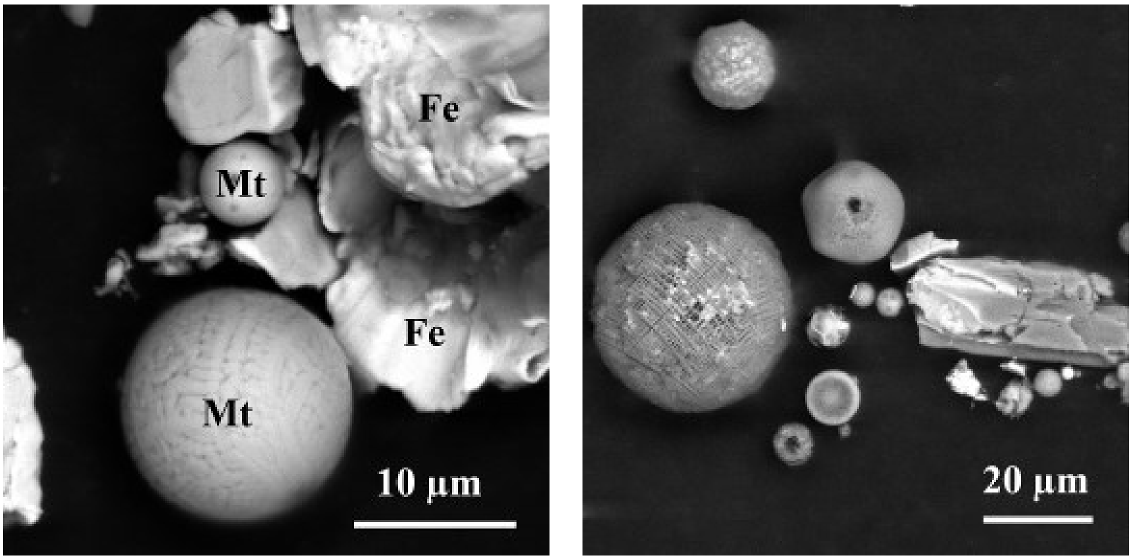


a) b)

**Fig.1.** General view of magnetic microparticles: magnetite and aluminosilicate microspheres, flake iron, clastic terrigenous magnetite.

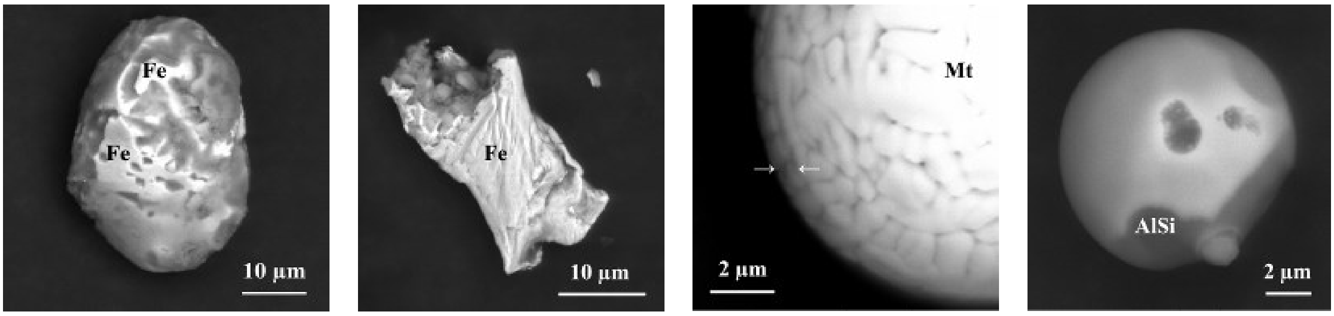


a) b) c) d)

**Fig.2.** Particles that could be formed as a result of thermal shock are shown: a) – a film of thermal shock origin on a Mt microspheres; b), c) – iron films, island and continuous; d) Mt film on aluminosilicate grain.

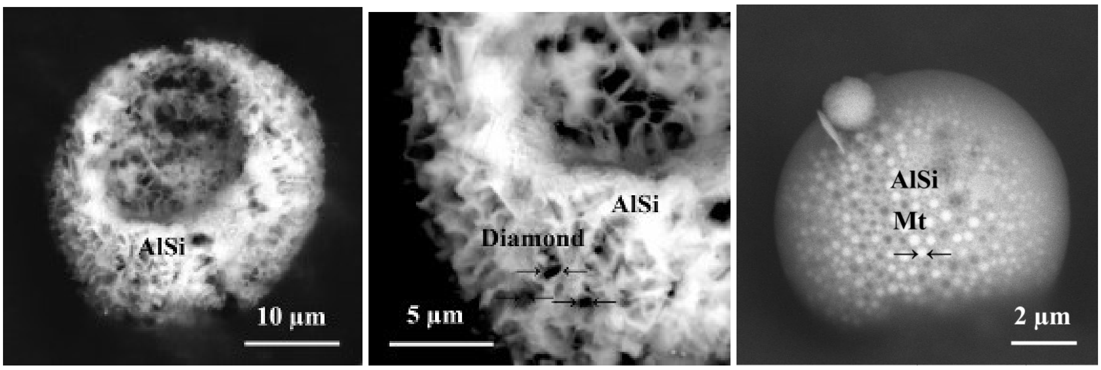


a) b) c)

**Fig.3.** Framework aluminosilicate with nanodiamond precipitates: a) general view b) fragment; c) a multi-level, complex system of aluminosilicate with Mt nanospheres.

Figure 3 shows a framework aluminosilicate with nanodiamond inclusions and a multi-level complex structure with magnetite inclusions. Figure 4 shows multi-level complex AlSi–$FeO_X$ systems with nanostructured precipitates that most likely arose during ultra-fast cooling after the explosion of the object. A multilevel complex $SiO_2$–$FeO_X$ system, similar to the one discovered, in (Kirillova, 2012).

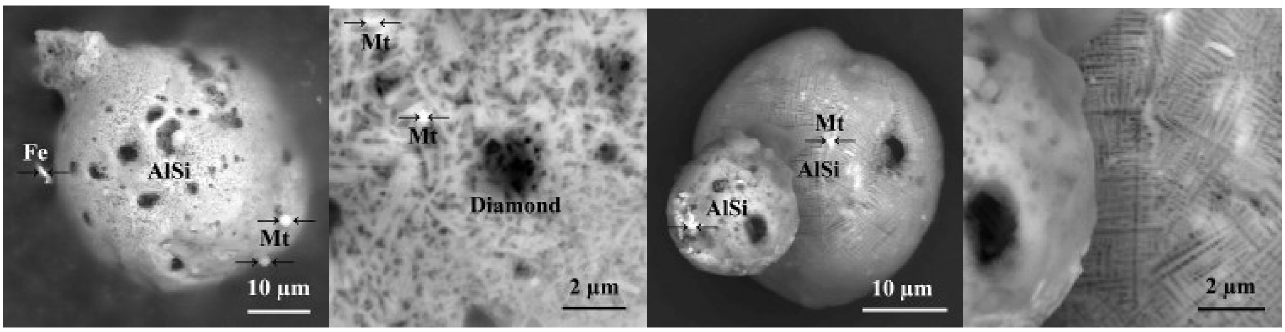


**Fig.4.** Multilevel complex AlSi–FeOx systems with nanostructured precipitates that arose during ultra-fast cooling after the explosion of the object.

**Discussion.** The study carried out in this work revealed that in the extracts from the samples that were taken at point 1 of the CCB "trace", there are indeed particles that differ in their special morphology, microstructure, and have an unusual complex composition. Among the particles isolated from the "trace" of CCB, aluminosilicate microspheres were found with a unique microstructure, transforming into nanostructural features that are not observed in particles formed during volcanic and technogenic processes (Kirillova, 2012; Mintova et al., 2015; Tosheva et al., 2012). The study of remanent saturation magnetization Irs did not reveal magnetic anomalies in the form of Irs bursts or others. This fact indicates the low density of the CCB material and the low content of magnetic particles in it, which also indicates the cometary nature of the CCB.

In the “trace” along the flight path and during the explosion of the CCB, water ice could not leave traces; the “traces” could be nano- and micro-particles of the CD deposited on the surface. Based on a set of differences found in the “trace” of microparticles, the authors believe that the Chulym bolide was most likely a fragment of a comet that had a solid-phase ice core and dust accompaniment.

**Conclusions.** When studying the objects found in the area of the CCB explosion, potentially its fragments, based on the sum of their characteristics, they were not classified as cosmogenic. The search for microparticles as “traces” of the fireball led to the discovery of microspheres with a special morphology, with micro-sized inclusions and nanostructures on their surface. The version of the cometary origin of the found microparticles, as formed as a result of the explosion of the CCB upon entering the dense layers of the atmosphere, according to the authors, is confirmed. Since it is the microparticles found in samples from the “trace”, and not macro-objects, that indicate the possible cometary nature of the CCB, this approach should be used in further research and the search for material evidence of the “cometitivity” of the Chulym bolide. The microporous formations and nano-sized inclusion crystals that we discovered on the microspheres are distinctive features at the micro- and nano-level, respectively, they can be considered as distinctive and diagnostic when assessing whether they belong to cometary material.

The work was carried out within the framework of the state assignment of the Institute of Physical Sciences of the Russian Academy of Sciences (No. FMWU-2022-0026, FMWU-2022-0027)

**References**

1. Voitsekhovsky A.I. The culprit of earthly troubles? Question Mark 1990. 48 pp.
2. Kirillova S.A., Almyashev V.I.. Formation of complex nanostructures based on the FeOx–SiO2–TiO2 system//Nanosystems: physics, chemistry, mathematics, 3:6 (2012), p. 98–104.
3. Levasseur-Regourd Anny-Chantal, Agarwal Jessica, Cottin Hervé, Engrand Cécile, Flynn George, Marco Fulle, Tamas Gombosi, Yves Langevin, Jérémie Lasue, Thurid Mannel, Sihane Merouane, Poch Olivier, Thomas Nicolas, Westphal Andrew. Cometary Dust //Space Sci Rev (2018) 214:64 https://doi.org/10.1007/s11214-018-0496-3
4. Mintova Svetlana, Jaber Maguy and Valtchev Valentin. Nanosized microporous crystals: emerging applications // Chem. Soc. Rev., 2015, 44, 7207 DOI:10.1039/C5CS00210A
5. Tosheva L., Brockbank A., Mihailova B., Sutula J., Ludwig J., Potgiete H., and Verran J. Micron and nanosized FAU-type zeolites from fly ash for antibacterial applications. //Journal of Materials Chemistry, September 2012, 22(33):16897 – 16905 DOI:10.1039/C2JM33180B
6. Tselmovich V.A., Amelin I.I., Gusiakov V.K., Kirillov V.E., Kurazhkovskiy A.Y. On the Possible Cometary Nature of the Uchur Cosmic Body (Fall 3.08. 1993) //Advances in Geological and Geotechnical Engineering Research, 2023. Vol. 05, Issue 03, P.16–24, https://doi.org/10.30564/agger.v5i3.5705 https://journals.bilpubgroup.com/index.php/agger/article/view/5705/4918.

## Yakovlev O.I., Shornikov S.I. Evaporation features of the outer zones of Ca–Al–inclusions of chondrites

V. I. Vernadsky Institute of Geochemistry & Analytical Chemistry RAS, Moscow (sergey.shornikov@gmail.com)

**Abstract.** The evaporation of CAIs type B was studied using the Knudsen effusion mass spectrometric method. It is shown that a complete disappearance of magnesium components is observed at temperatures above 2200 K, while the silicon components remain in the CAIs melt. This observation corresponds to the disappearance of spinel and other magnesium-containing minerals during crystallization of the residual melt on the rims of CAIs subtype B1. In turn, an increase of the $Al_2O_3$ content in the residual melt due to spinel decay and magnesium evaporation leads to an increase of the content of gehlenite in melilite, which is also observed at the edges of the high-temperature zone of the rims of the CAIs subtype B1.

***Keywords***: *Ca–Al–inclusions of chondrites, evaporation, Knudsen effusion mass spectrometric method*

Ca–Al inclusions of chondrites (CAIs) are unique objects of meteoritics. They were formed as a result of complex processes of condensation and evaporation of a substance of presumably Solar composition. There are several types of inclusions that differ in composition (A, B, C). Type B is structurally divided into subtypes B1 and B2.

Subtype B1 contains zones of the central core and mantle melilite, consisting mainly of spinel ($MgAl_2O_4$), melilite (a mineral of the series akermanite $Ca_2MgSi_2O_7$ – gehlenite $Ca_2Al_2SiO_7$) and fassaite (diopside with a high content of $Al_2O_3$ and $TiO_2$), and an external monomineral rim consisting of melilite rich in gehlenite (Fig. 1). The typical profile of akermanite and $\delta^{25}$Mg between the core and rim zones in CAI of subtype B1 (Allende 5241) according to the data (Kerekgyarto et al., 2016) is shown in Fig. 1. Subtype B2 is similar in mineral composition to the core zone of subtype B1.

As follows from Fig. 1, the akermanite content in the core zone of the inclusion is approximately 50 wt. %, the akermanite content drops to 20 wt. % in the mantle melilite zone, and up to 7 wt. % in the rim zone. A decrease in the akermanite content in the profile under consideration corresponds to an increase in the $^{25}Mg$ heavy isotope, that indicated the course of evaporative processes.

Based on experimental data obtained by the Knudsen effusion mass spectrometric method for evaporation of CAIs type B substance (Shornikov, Yakovlev, 2022), it can be assumed that the reason for the structural difference between CAIs subtypes B1 and B2 is in the predominant evaporation and removal of magnesium from the melt at temperatures above 2200 K while preserving the silicon component in the melt. It follows from the temperature dependencies of the partial pressures of the vapor species prevailing in the gas phase, corresponding to the MgO and $SiO_2$ content in the residual melt – $p_{Mg}$ and $p_{SiO}$ (Fig. 2A).

Based on determined oxide activities ($a_i$) in the residual CAI type B melt during evaporation (Fig. 2B), the spinel, akermanite and gehlenite activities in the melt can be calculated. The oxide activities in melts of the «pure» compounds were taken from data obtained in (Shornikov et al., 1996; Bale et al., 2016; Shornikov, 2017).

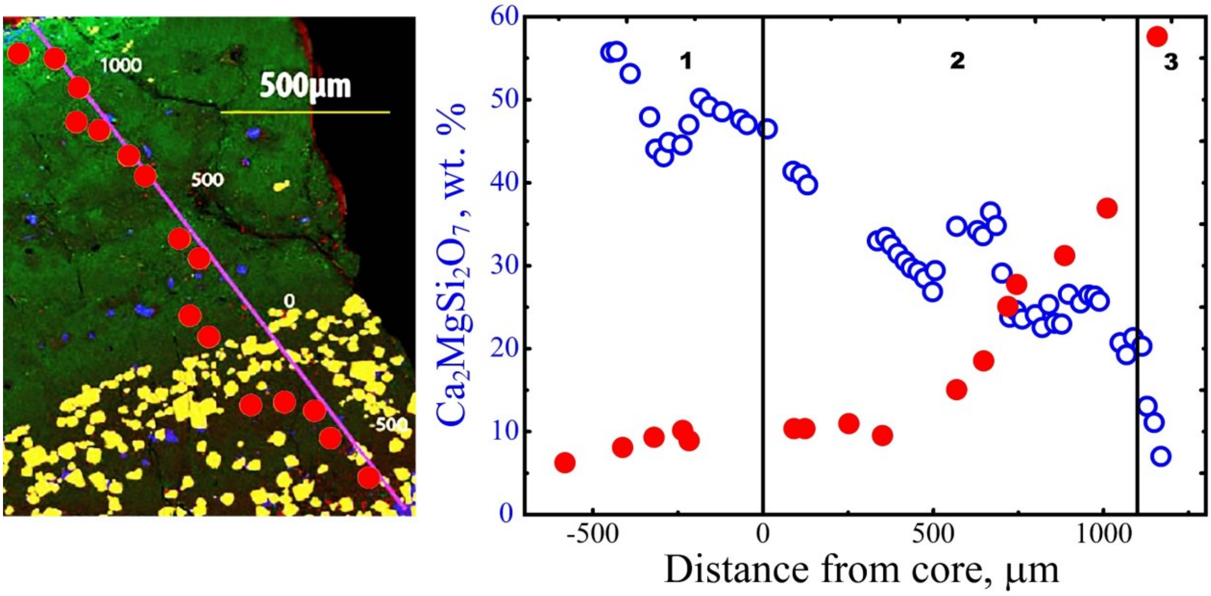


**Fig. 1.** Experimental profiles of akermanite and $\delta^{25}Mg$ in the core (1), mantle melilite (2) and rim (3) zones in CAI type B1 (Kerekgyarto et al., 2016).

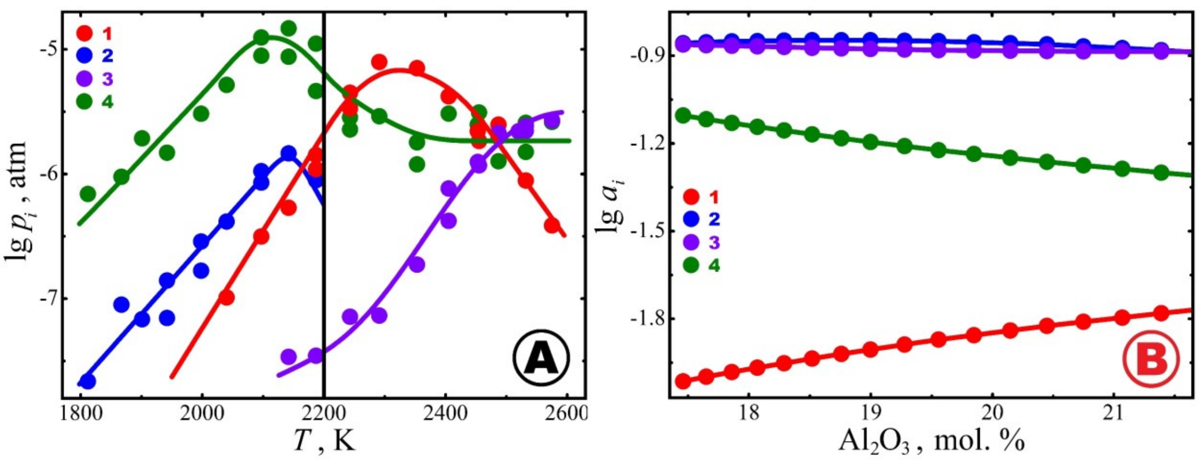


**Fig. 2.** (A) The partial pressures of the Ca (1), Mg (2), Al (3) and SiO (4) vapor species over the CAI type B melt during evaporation from the Knudsen effusion cell and (B) the CaO (1), MgO (2), $Al_2O_3$ (3) and $SiO_2$ (4) activities in the CAI type B residual melt during evaporation.

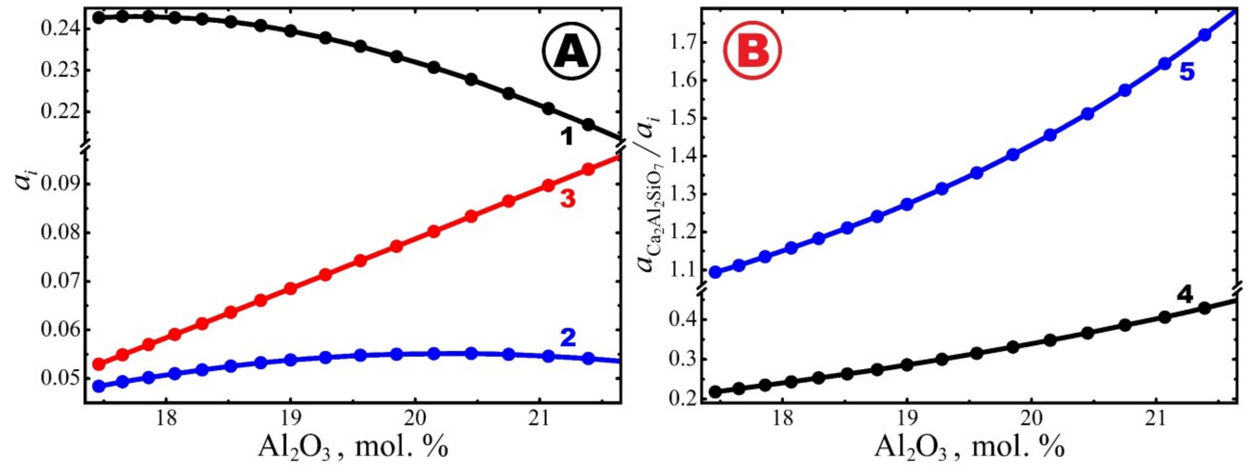


**Fig. 3.** (A) The $MgAl_2O_4$ (1), $Ca_2MgSi_2O_7$ (2) and $Ca_2Al_2SiO_7$ (3) activities, as well as (B) their ratios of $Ca_2Al_2SiO_7$ / $MgAl_2O_4$ (4) and $Ca_2Al_2SiO_7$ / $Ca_2MgSi_2O_7$ (5) in the CAI type B residual melt during evaporation.

Based on the Lewis relations (Lewis & Randall, 1923), the following expressions can be written for the activities of compounds in the residual melt:

$$a^{melt}_{MgAl_2O_4} = \frac{p^{melt}_{MgAl_2O_4}}{p^{spin}_{MgAl_2O_4}} = \frac{a^{melt}_{MgO} a^{melt}_{Al_2O_3}}{a^{spin}_{MgO} a^{spin}_{Al_2O_3}} \quad (1)$$

$$a^{melt}_{Ca_2MgSi_2O_7} = \frac{p^{melt}_{Ca_2MgSi_2O_7}}{p^{aker}_{Ca_2MgSi_2O_7}} = \frac{(a^{melt}_{CaO})^2 a^{melt}_{MgO} (a^{melt}_{SiO_2})^2}{(a^{aker}_{CaO})^2 a^{aker}_{MgO} (a^{aker}_{SiO_2})^2} \quad (2)$$

$$a^{melt}_{Ca_2Al_2SiO_7} = \frac{p^{melt}_{Ca_2Al_2SiO_7}}{p^{gehl}_{Ca_2Al_2SiO_7}} = \frac{(a^{melt}_{CaO})^2 a^{melt}_{Al_2O_3} a^{melt}_{SiO_2}}{(a^{gehl}_{CaO})^2 a^{gehl}_{Al_2O_3} a^{gehl}_{SiO_2}}, \quad (3)$$

where the activities and pressures of oxides with the «*melt*» index correspond to those in the residual melt, and the activities and pressures of oxides with the «*spin*», «*aker*» and «*gehl*» indices correspond to those in the spinel, akermanite and gehlenite melts (at the same temperature).

From Fig. 3A, it is possible to notice a tendency to decrease the spinel and akermanite activities with an increase in the gehlenite activity during the melt evaporation (characterized by an increase in the $Al_2O_3$ content), which becomes noticeable when comparing their ratios (Fig. 3B). This observation confirms the distribution of magnesium-containing mineral forms in the profile shown in Fig. 1 (Kerekgyarto et al., 2016).

Selective evaporation of magnesium led to the disappearance of substances in the Ca–Al–inclusions from the outer molten zone of magnesium-containing minerals – spinel and fassaite. At the same time, an increase in the $Al_2O_3$ content and, accordingly, gehlenite in melilite occurred in the melt. Melting and evaporation in the outer zone of subtype B1 could occur in the protosolar system during the so-called «flash heating» process.

Thus, when CAIs type B evaporates at temperatures above 2200 K, a complete disappearance of magnesium is observed while the silicon component remains in the melt. In this case, spinel and other magnesium-containing minerals do not crystallize in the residual melt, which is observed in the CAIs rim zone of subtype B1. At the same time, in the residual melt, due to the decay of spinel and evaporation of magnesium, the $Al_2O_3$ content increases, that, in turn, leads to an increase in the gehlenite content in melilite, which is also observed at the edges of the high-temperature zone of the CAIs subtype B1 rim.

### References

Bale C.W., Belisle E., Chartrand P., Decterov S.A., Eriksson G., Gheribi A.E., Hack K., Jung I.-H., Kang Y.-B., Melancon C., Pelton A.D., Petersen S., Robelin C., Sangster J., Spencer P., Van Ende M-A. (2016) FactSage thermochemical software and databases, 2010–2016. *CALPHAD*, vol. 54, pp. 35–53.

Kerekgyarto A. G., Jeffcoat C. R., Lapen T. J., Andreasen R., Righter M., Ross D. K., Simon J. I. (2016) Al-Mg isotope study of Allende 5241. *47th Lunar & Planet. Sci. Conf*., Abs. #3041.

Lewis G.N., Randall M. (1923) Thermodynamics and the free energy of chemical substances. N. Y., McGraw-Hill, 653 p.

Shornikov S. I., Stolyarova V. L., Shultz M. M. (1996) Mass spectrometric study of thermodynamic properties of the $CaO–Al_2O_3–SiO_2$ melts. *Technique & Technology of Silicates*, vol. 3, № 1–2, pp. 8–22.

Shornikov S. I. (2017) Thermodynamic properties of spinel $MgAl_2O_4$: a mass spectrometric study. *Russ. J. Phys. Chem. A*, vol. 91, № 2, pp. 287–294.

Shornikov S. I., Yakovlev O. I. (2022) Mass spectrometric study of the evaporation of CAIs melts (types A and B) of the Efremovka meteorite. *Physico-chemical & Petrophysical Research in Earth Sciences (XXIII)*, Moscow, IGEM RAS, pp. 320–323.